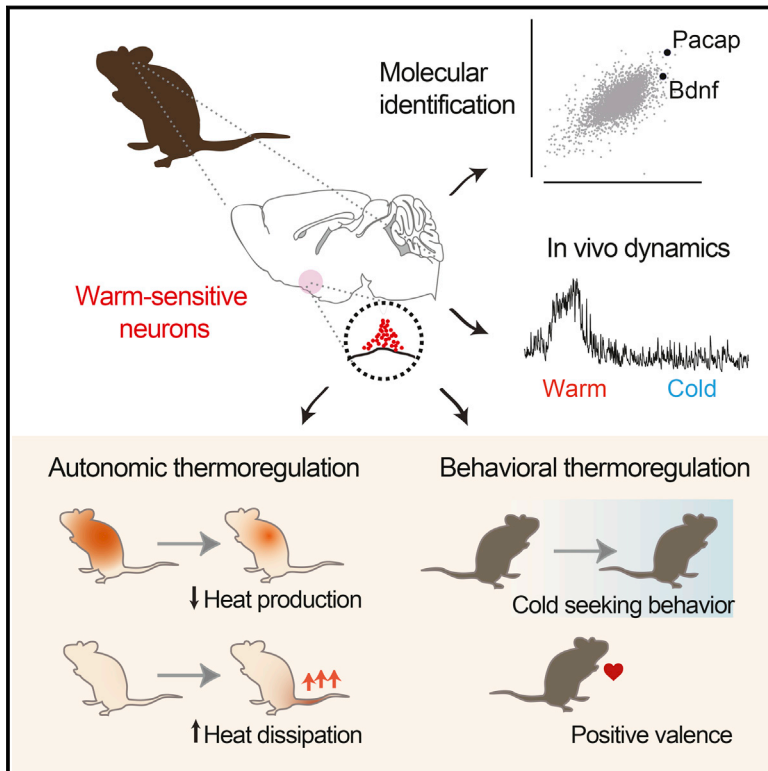# Warm-Sensitive Neurons that Control Body Temperature

Graphical Abstract

Authors

Chan Lek Tan, Elizabeth K. Cooke, David E. Leib, Yen-Chu Lin, Gwendolyn E. Daly, Christopher A. Zimmerman, Zachary A. Knight

Correspondence

zachary.knight@ucsf.edu

In Brief

A specific population of neurons regulates body temperature in mammals by coordinating the behavioral and autonomic response to heat.

Highlights

- Preoptic neurons co-expressing BDNF/PACAP are rapidly activated by ambient warmth

- Stimulation of these warm-sensitive neurons (WSNs) rapidly reduces body temperature

- WSNs activate a coordinated program of autonomic and behavioral responses to heat

- WSN projections delineate the structure of the downstream thermoregulatory circuit

Data Resources

GSE80121
GSE80120
GSE80224

CrossMark

CellPress

Article

Warm-Sensitive Neurons that Control Body Temperature

Chan Lek Tan,[1,2] Elizabeth K. Cooke,[1,2] David E. Leib,[1,2,3] Yen-Chu Lin,[1,2] Gwendolyn E. Daly,[1,2] Christopher A. Zimmerman,[1,2,3] and Zachary A. Knight[1,2,3,4,*]
[1]Department of Physiology
[2]Kavli Institute for Fundamental Neuroscience
[3]Neuroscience Graduate Program
University of California, San Francisco, San Francisco, CA 94158, USA
[4]Lead Contact
*Correspondence: zachary.knight@ucsf.edu
http://dx.doi.org/10.1016/j.cell.2016.08.028

SUMMARY

Thermoregulation is one of the most vital functions of the brain, but how temperature information is converted into homeostatic responses remains unknown. Here, we use an unbiased approach for activity-dependent RNA sequencing to identify warm-sensitive neurons (WSNs) within the preoptic hypothalamus that orchestrate the homeostatic response to heat. We show that these WSNs are molecularly defined by co-expression of the neuropeptides BDNF and PACAP. Optical recordings in awake, behaving mice reveal that these neurons are selectively activated by environmental warmth. Optogenetic excitation of WSNs triggers rapid hypothermia, mediated by reciprocal changes in heat production and loss, as well as dramatic cold-seeking behavior. Projection-specific manipulations demonstrate that these distinct effectors are controlled by anatomically segregated pathways. These findings reveal a molecularly defined cell type that coordinates the diverse behavioral and autonomic responses to heat. Identification of these warm-sensitive cells provides genetic access to the core neural circuit regulating the body temperature of mammals.

INTRODUCTION

Prolonged deviations in core body temperature outside a narrow range are incompatible with life, and consequently, body temperature is tightly regulated by a homeostatic system (Morrison and Nakamura, 2011). In response to cold or warmth, the brain triggers an array of counter regulatory responses that defend body temperature against change. These responses include both autonomic effectors such as thermogenesis, vasodilation, and sweating, as well as behavioral mechanisms that trigger flexible, goal-oriented actions, such as warm- or cold-seeking, nest building, and putting on clothing.

How the brain coordinates these diverse effector mechanisms in order to achieve body temperature stability is a longstanding and unresolved question. Classical models posited the existence of a central integrator in the brain that senses temperature signals, compares them to a set point, and then orchestrates the homeostatic response (Hammel, 1968). In contrast, more recent theories propose that the brain has no central integrator for body temperature; instead, thermoregulatory effectors are thought to be regulated independently, giving the appearance of coordinated action without the existence of a controller (McAllen et al., 2010; Romanovsky, 2007; Satinoff, 1978). Discriminating between these models has fundamental implications for our understanding of how the brain gives rise to homeostasis, yet at present these ideas remain speculative due to the lack of information about the underlying neural substrates. Progress toward addressing these questions will require a deeper understanding of the cells and circuits that mediate thermoregulation.

The preoptic area (POA) of the hypothalamus has traditionally been the brain region most strongly associated with thermoregulation (Hammel, 1968). Classical experiments showed that non-targeted stimulation of the POA could trigger dramatic thermoregulatory responses, such as panting and sweating, that were "in all points similar to those obtained by heating the entire animal" (Magoun et al., 1938). Lesioning of this structure had the opposite effect, abolishing thermoregulatory responses in animals subjected to temperature challenge (Clark et al., 1939; Teague and Ranson, 1936). Electrophysiologic recordings revealed that the POA contains a subset of neurons that are activated by local or environmental heat and therefore are "warm-sensitive" (Boulant and Hardy, 1974; Hardy et al., 1964; Nakayama et al., 1961).

Based on these and other observations, the POA has long been thought to play a critical role in thermoregulation. Yet how the POA performs this function remains unclear, because its underlying neural circuitry is poorly defined. The POA is a highly heterogeneous structure, containing intermingled cell types that mediate distinct processes such as sleep, mating, parental behaviors, and fluid and cardiovascular homeostasis (McKinley et al., 2015; Scott et al., 2015; Wu et al., 2014). It remains unclear how to identify the key thermoregulatory cell types in the POA, how those cells are regulated, where their axons

project, and which effector mechanisms they control (Morrison and Nakamura, 2011; Nagashima et al., 2000).

We reasoned that molecular identification of thermoregulatory neurons in the POA would provide a genetic entry point into this circuitry, thereby enabling targeted functional analysis of the neural circuit that controls body temperature. Here, we report the unbiased identification of a molecularly defined population of preoptic neurons that are rapidly and selectively activated by environmental warmth. We show that activation of these cells is sufficient to orchestrate the coordinated homeostatic response to heat, including both its autonomic and behavioral components. We show that through their axon projections these warm-sensitive neurons delineate the structure of the downstream circuit, revealing new brain regions not previously implicated in thermoregulation. These findings identify a central convergence point for the regulation of body temperature in the brain and open the door to systematic genetic dissection of the thermoregulatory circuit.

RESULTS

Molecular Identification of Preoptic Warm-Sensitive Neurons

To identify thermoregulatory neurons in the hypothalamus, we used an unbiased approach for the molecular profiling of activated neurons termed phosphoTRAP (Knight et al., 2012). This method takes advantage of the fact that neural activation results in phosphorylation of ribosomal protein S6, which is a structural component of the ribosome. These phosphorylated ribosomes can be captured from mouse brain homogenates, thereby enriching for the mRNA selectively expressed in neurons activated by a stimulus (Figure 1A). This captured mRNA can then be sequenced to reveal the molecular identity of the activated cells (Knight et al., 2012).

We challenged mice with exposure to environmental warmth (37°C) and then performed immunostaining for pS6 in brain slices. Warm-challenge induced prominent pS6 within a discrete population of neurons within the anterior ventromedial preoptic area (VMPO) (Figures 1B and 1C). This pattern of pS6 induction resembled previous reports of Fos expression in response to warmth (Scammell et al., 1993; Yoshida et al., 2005), but was anatomically distinct from preoptic pS6 induced by cold-challenge (Figures S1B and S1C) or food deprivation (Knight et al., 2012).

To identify these putative warm-sensitive neurons, we challenged mice with heat, immunoprecipitated (IP) pS6 ribosomes from homogenates of the microdissected anterior hypothalamus, and then sequenced this RNA to determine the fold-enrichment for each gene (pS6 IP/Input; Figure 1A). As expected, the most highly enriched transcripts included numerous immediate early genes, such as Fos (Figure 1D, red). The enrichment of these genes confirms that the pS6 IP selectively isolated mRNA from activated neurons (Knight et al., 2012). In addition, we identified a number of genes with restricted expression patterns that could potentially label the warm-activated cells (Figure 1D, blue). Among these, two of the most highly enriched were the neuropeptides pituitary adenylate cyclase-activating polypeptide (Adcyap1, also known as PACAP; 10.5-fold) and

brain-derived neurotrophic factor (Bdnf; 8.7-fold). Analysis of the expression pattern of these genes revealed striking resemblance to the pattern of pS6 induction following warm-challenge (Figures 1E and S1), suggesting these markers may specifically identify preoptic warm-sensitive neurons.

To gain genetic access to these cells, we generated knockin mice expressing Cre recombinase from the Bdnf locus (BDNF-2A-Cre) (Figures 1J and S1G–S1M) and obtained an analogous PACAP-2A-Cre line (Harris et al., 2014). We used these Cre drivers to label BDNF and PACAP neurons with GFP (Figure 1E) and then quantified the co-localization between GFP and warm-activated pS6. Consistent with RNA sequencing (RNA-seq) data, approximately two-thirds of warm-induced pS6$^+$ neurons colocalized with BDNF and PACAP in the VMPO (Figures 1F and 1G), whereas approximately half of PACAP and BDNF neurons were pS6$^+$ (Figures 1F and 1H). By contrast, there was very little overlap between cold-induced pS6 and either marker (Figures S1D and S1E). This degree of specific colocalization between warm-induced pS6 and BDNF/PACAP is comparable to the overlap between markers of known hypothalamic cell types and Fos expression in response to their cognate stimuli (Knight et al., 2012; Lee et al., 2014; Wu et al., 2014), suggesting that these neuropeptides may usefully identify warm-activated thermoregulatory neurons.

To determine whether BDNF and PACAP are expressed in the same neurons, we quantified their colocalization in the VMPO using Cre and LacZ reporter strains. More than 90% of BDNF neurons expressed PACAP, whereas ~80% of PACAP neurons expressed BDNF (Figure 1I). Thus, these two genes delineate primarily a single population of neurons representing a subset of cells within the VMPO (Figure S1F). To further characterize the molecular identity of these BDNF/PACAP neurons, we purified mRNA from each cell population via TRAP (Heiman et al., 2014) and then performed deep sequencing of their transcriptomes (Figure 1K). As expected, Bdnf was among the most highly enriched genes in PACAP expressing neurons, and vice versa, confirming that these genes are expressed in highly overlapping cells (Figure 1L). In addition, we identified neuropeptides (Unc3, Nxph4, Ghrh), transcription factors (Emx2, Fezf1, Nhlh2), and receptors (Brs3) that are selectively expressed in these putative warm-activated cells and may contribute to their function (Table S1). Conversely, we observed no enrichment for genes that label known populations of preoptic neurons, such as galanin (Wu et al., 2014), tyrosine hydroxylase (Scott et al., 2015), the leptin receptor (Zhang et al., 2011), and gonadotropin releasing-hormone (Suter et al., 2000). Thus, BDNF and PACAP identify a highly overlapping population of neurons within the VMPO that is distinct from known preoptic cell types and is biochemically activated by ambient warmth.

Natural Dynamics of Warm-Sensitive Neurons

To investigate how VMPO$^{PACAP/BDNF}$ neurons are regulated in vivo, we used fiber photometry (Gunaydin et al., 2014) to record their natural dynamics in awake, behaving mice (Figures 2A and 2B). We targeted the calcium reporter GCaMP6s to VMPO$^{PACAP/BDNF}$ neurons by injection of a Cre-dependent AAV into the VMPO of PACAP-2A-Cre mice. In slice recordings, GCaMP6s faithfully reported VMPO^{PACAP} neuron activity
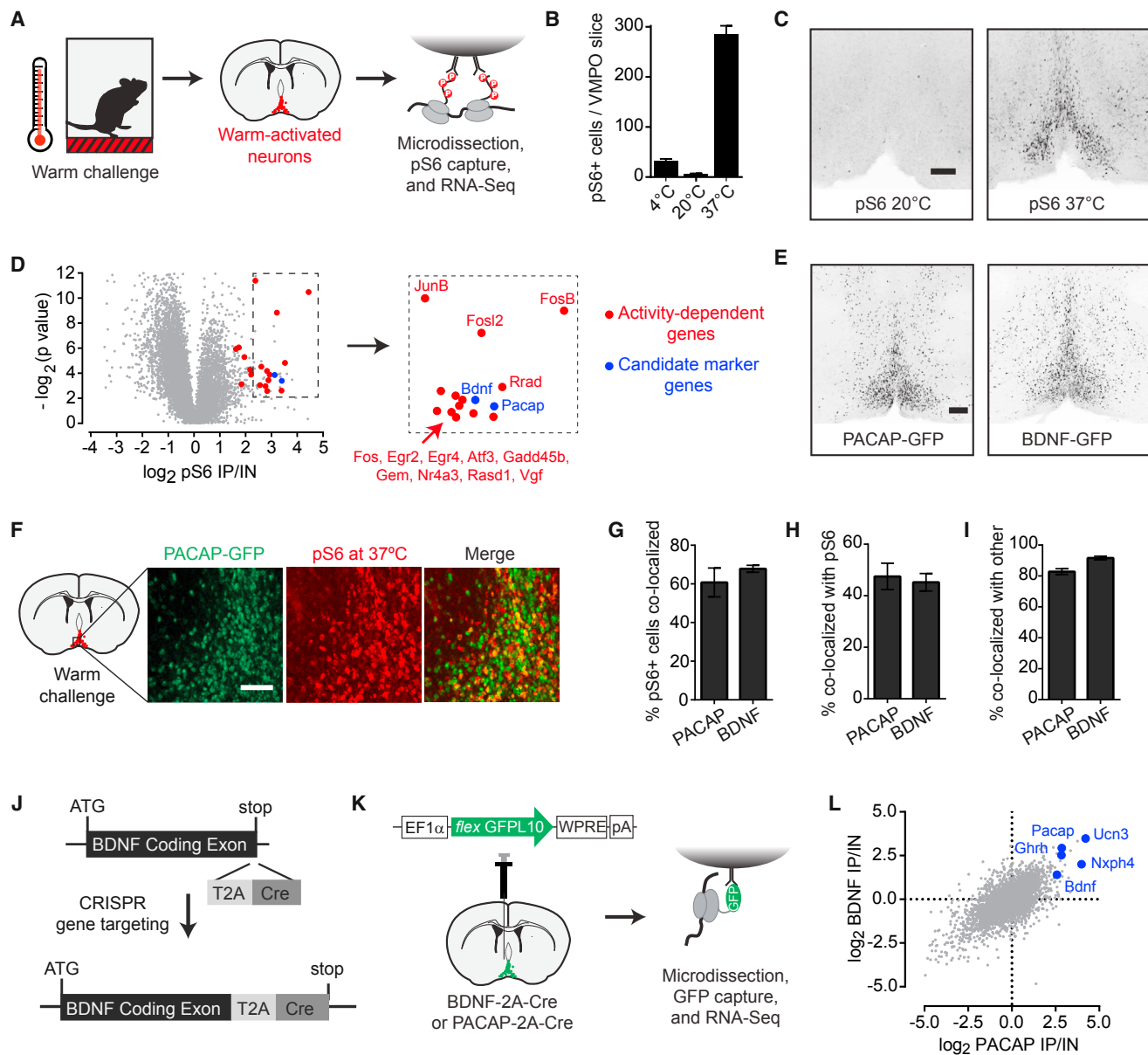
Figure 1. Warm-Activated POA Neurons Express PACAP and BDNF

(A) PhosphoTRAP strategy for genetic identification of warm-activated neurons.

(B) Number of activated (pS6$^+$) cells in the VMPO after subjecting mice to warm (37°C), cold (4°C), or regular ambient temperatures.

(C) Anatomic location of pS6-positive cells after warm exposure. Scale bar, 200 μm.

(D) PhosphoTRAP sequencing results. Fold enrichment in IP versus input fraction (x axis) and statistical significance (y axis) are shown. Blue: candidate markers of activated neurons; Red: activity-induced immediately early genes. Microdissected preoptic area from five to eight animals were pooled in each of the three experimental replicates.

(E) Distribution of PACAP and BDNF neurons in the VMPO based on Cre-dependent GFP reporter expression. Scale bar, 200 μm.

(F) Colocalization of PACAP-GFP (green) with warm-activated pS6 (red). Scale bar, 200 μm.

(G and H) Bar graphs quantifying colocalization of warm-activated pS6 with GFP expressed in either PACAP- (Pac) or BDNF-expressing cells. (G) Percentage of pS6$^+$ neurons that are GFP$^+$. (H) Percentage of GFP$^+$ neurons that are pS6$^+$. n = 3 per group.

(I) Percentage of PACAP-GFP neurons positive for BDNF-LacZ (Pac) and vice-versa (BDNF). n = 3 per group.

(J) CRISPR-aided generation of Cre-knock in allele at the endogenous BDNF locus.

(K and L) RNA-seq profiling of selective gene expression in PACAP or BDNF neurons using TRAP. (K) Schematic of TRAP strategy. Microdissected preoptic area from six to ten animals were pooled in each experimental replicate. Two experimental replicates each were performed for PACAP-Cre-labeled neurons and for BDNF-Cre-labeled neurons. (L) Scatter plot showing fold-enrichment of each gene in BDNF neurons (y axis) or in PACAP neurons (x axis). Selected neuropeptide genes are highlighted in blue.

Values are reported as mean ± SEM. See also Figure S1.
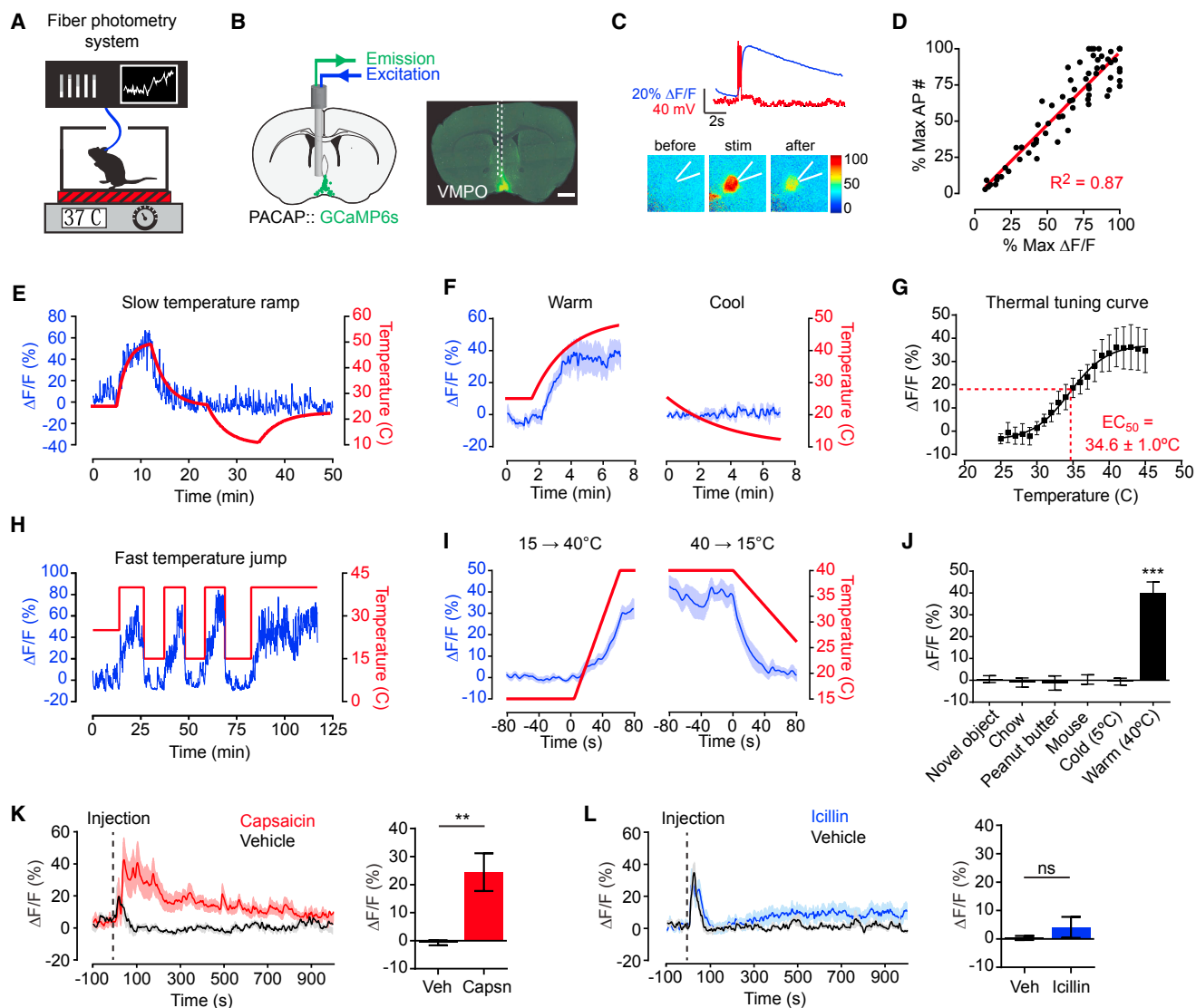
Figure 2. Natural Dynamics of VMPO[PACAP] Neurons

(A) Fiber photometry setup to record VMPO[PACAP] neural activity in awake animals in response to temperature changes.

(B) Schematic and representative coronal section show placement of optical fiber above VMPO[PACAP] neurons expressing GCAMP6s (green). Scale bar, 500 μm.

(C) Fluorescence increase (blue line) and action potential spikes (red) in response to current injection in representative VMPO[PACAP] cell.

(D) GCAMP6s fluorescence signal increases proportionally with induced action potential spikes. n = 7 mice.

(E) Representative trace recorded during gradual temperature ramps between 47°C and 10°C.

(F) Mean responses during gradual temperature changes from 25°C to 47°C (Warm) or from 25°C to 10°C (Cool). n = 5, one-way repeated measures (RM)-ANOVA, $F_{20,140}$(warm) = 15.2, p < 0.001; $F_{14,56}$(cool) = 1.09, p = 0.38.

(G) Mean response at each 1°C temperature interval during gradual temperature ramp experiments. n = 8. Fitted curve with 4-PL, sigmoidal function is shown.

(H) Representative trace recorded during rapid temperature steps between 40°C and 15°C.

(I) Mean responses during rapid temperature transitions shown in (H). n = 7.

(J) Mean response during first 1,000 s following exposure to each stimulus. n = 6. ***p < 0.001, Bonferroni multiple comparisons test on all possible pairs.

(K and L) Fluorescence response to capsaicin (K) or icilin (L) injection normalized to paired responses to vehicle injection. Animal handling and Injection starts at time = 0. Bar graphs show average response in 5-min window after vehicle/drug injection. Two-tailed paired t test versus vehicle: capsaicin p = 0.0093, icilin p = 0.34. n = 9.

Values are reported as mean ± SEM. See also Figure S2.

induced by current injection (Figures 2C and 2D). We then installed an optical fiber above the VMPO for photometry recordings in vivo (Figures 2A and 2B).

We tested mice in a custom-built chamber that enables rapid temperature control (Figure 2A). Increasing the ambient temperature from 25°C to 45°C resulted in a progressive increase in

calcium signals (Figures 2E and 2F), demonstrating that VMPO^{PACAP} neurons are warm-activated in vivo. Slow temperature ramps (Figures 2E and 2F) and rapid temperature steps (Figures 2H and 2I) yielded similar increases in total fluorescence, indicating that absolute temperature (rather than the rate of change) primarily determines the activity response. Consistent with this, prolonged warm exposure caused calcium signals to remain stably elevated for the duration of the heat challenge (tens of minutes; Figures S2J and S2K). We generated a thermal tuning curve for these cells by measuring calcium signals at one degree increments, which was fit by a sigmoidal function with an EC$_{50}$ of 34.6°C ± 1.0°C (Figure 2G). This temperature sensitivity overlaps with the range of innocuous warmth over which heat defensive autonomic responses are normally activated (Crane et al., 2014; Garami et al., 2011). Thus, VMPO^{PACAP} neurons are activated by environmental warmth at temperatures that trigger natural thermoregulatory responses, as would be predicted for neurons with a specialized function in body temperature control.

VMPO^{PACAP} neurons responded to ambient warmth within seconds (Figure 2I), which is consistent with regulation by heat-activated thermoreceptors in the skin rather than slower changes in core body temperature. This rapid warm-activation was highly specific to VMPO^{PACAP} neurons, since no response to ambient heat was observed in photometry recordings from an adjacent but distinct population of preoptic neurons expressing galanin (POA^{GAL}) (Figures S2D–S2F); in recordings from an unrelated population of homeostatic neurons that control thirst (SFO^{NOS1}) (Figures S2G–S2I); or in recordings from VMPO^{PACAP} neurons expressing GFP in place of GCaMP6s (Figures S2A–S2C).

The thermosensitivity of VMPO^{PACAP} neurons was tightly restricted to the range of innocuous warmth, as neither transient reductions in environmental temperature below 25°C nor prolonged cold exposure (5°C) caused any change in calcium signals from these cells (Figures 2E, 2F, S2J, and S2K). Consistent with this warm-sensitivity, VMPO^{PACAP} neurons were strongly activated by peripheral challenge with capsaicin, an agonist of the heat-sensitive ion channel TRPV1 (Figure 2K), but were unaffected by treatment with icilin, an agonist of the cold-sensitive channel TRPM8 (Figure 2L) (Caterina et al., 1997; McKemy et al., 2002). This insensitivity to icilin was observed even when VMPO^{PACAP} neurons were preactivated by exposure to ambient heat (Figures S2N and S2O). Thus, VMPO^{PACAP} neurons are selectively regulated by signals arising from a subset of heat-activated sensory fibers expressing TRPV1, but not the corresponding cold-activated fibers expressing TRPM8. In contrast to these responses to thermal signals, we observed no response to a range of unrelated stimuli, including food presentation and consumption, novel objects, and social interactions with other mice (Figure 2J). Taken together, these data show that VMPO^{PACAP} neurons are specifically and rapidly regulated by the peripheral detection of environmental warmth, consistent with a functional role for these neurons in the homeostatic response to heat.

Warm-Sensitive Neurons Control Autonomic Responses to Heat

The rapid activation of POA^{PACAP} neurons by ambient warmth suggests that these cells may contribute to thermoregulatory responses. To test their causal role, we used an optogenetic sensitizer to replay this natural activation in awake, behaving mice. We targeted expression of a stabilized step function opsin (Yizhar et al., 2011) (SSFO) to these cells by injection of a Cre-dependent AAV into the VMPO of PACAP and BDNF Cre driver mice (Figure 3A). SSFOs promote long-lasting increases in neural excitability (~30 min) in response to brief light stimulation (~30 s) and thus minimize local tissue heating that accompanies sustained light delivery (Stujenske et al., 2015). This consideration was critical for these experiments because the POA contains intrinsically thermosensitive neurons (Hardy et al., 1964; Magoun et al., 1938; Nakayama et al., 1961). An additional advantage of SSFOs is that they induce asynchronous firing that may mimic natural activity more closely than other modes of stimulation (Yizhar et al., 2011).

We first confirmed that SSFO activation induces stable, subthreshold depolarization of VMPO$^{PACAP/BDNF}$ neurons in vitro (Figures 3B and S3J–S3L). We then tested the effect of brief blue light stimulation (30 s, 10 mW, 2 Hz) on either opsin-expressing or control mice. Photostimulation triggered a rapid decline in core body temperature in mice expressing SSFOs in VMPO$^{PACAP/BDNF}$ neurons (Figure 3D, red and blue). This response to brief stimulation persisted for 30 min before core temperature fully returned to baseline, consistent with the kinetics of SSFO inactivation (Figure S3L) (Yizhar et al., 2011). Repeated photostimulation resulted in durable suppression of body temperature that persisted as long as the stimulation continued (>1 hr; Figure S3A, red). By contrast, control mice that lacked SSFO expression showed no body temperature change under any stimulation paradigm (Figures 3D and S3A, black). Pre-exposure of animals to ambient heat fully occluded the hypothermic effect of VMPO$^{PACAP/BDNF}$ neuron stimulation (Figures S3H and S3I), consistent with the fact that these neurons are activated by warmth (Figure 2J). Thus, activation of VMPO$^{PACAP/BDNF}$ neurons is sufficient to induce hypothermia, as would be predicted for bona fide warm-sensitive neurons.

We investigated the mechanism underlying this body temperature change. Two primary means of autonomic thermoregulation in rodents are tail vasodilation, which enables heat dissipation, and brown adipose tissue (BAT) thermogenesis, which enables heat production. To record these two parameters in awake animals, we imaged tail vasodilation by infrared thermography and monitored BAT thermogenesis by wireless telemetry. Stimulation of VMPO$^{PACAP/BDNF}$ neurons caused a striking increase in tail temperature (up to 6°C within 2 min), indicating robust activation of tail vasodilation (Figures 3C and 3E). In parallel, BAT temperature rapidly declined, indicating suppression of heat production (Figure 3F). This inhibition of BAT thermogenesis was observed even when mice were cold-challenged (Figures S3B and S3C), indicating that VMPO$^{PACAP/BDNF}$ neurons can override the natural cold-defensive response. Stimulation of VMPO$^{PACAP/BDNF}$ neurons had no effect on locomotion (Figures S3D–S3G), indicating that none of these thermoregulatory effects were secondary to changes in activity. Thus, VMPO$^{PACAP/BDNF}$ neurons reciprocally and specifically regulate two major autonomic mechanisms of thermoregulation, enabling a rapid decrease in core body temperature in response to heat challenge.
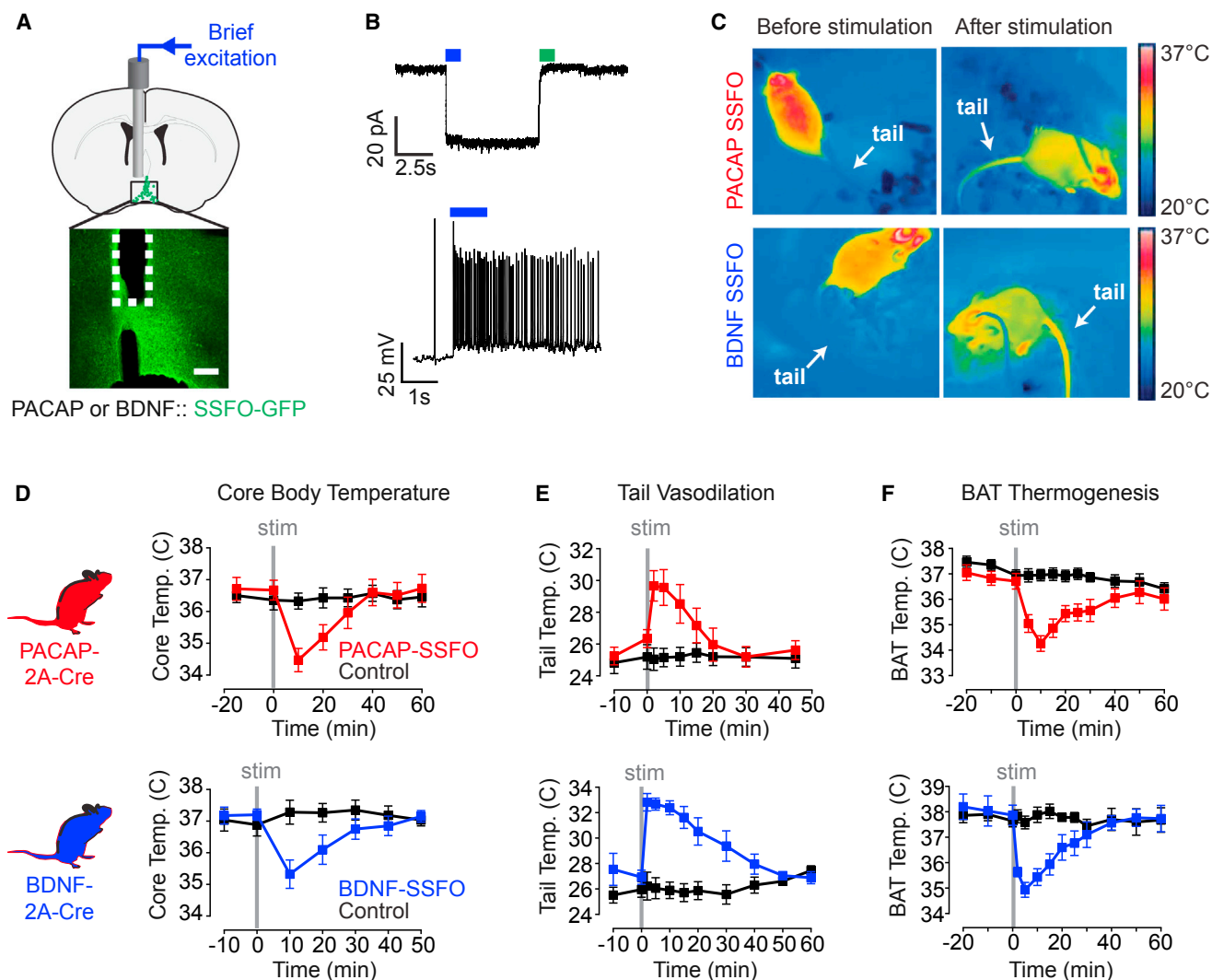
Figure 3. Optogenetic Activation of VMPO[PACAP/BDNF] Neurons Induces Hypothermia

(A) Schematic and representative slice showing placement of optical fiber above VMPO[PACAP/BDNF] neurons expressing SSFO-eYFP (green). Scale bar, 100 μm.

(B) Representative patch-clamp recording trace showing light-induced photocurrent (top) and action potentials (bottom) in VMPO[PACAP/BDNF] neurons expressing SSFO.

(C) Infrared thermography shows tail vasodilation (arrow) and trunk temperature loss upon VMPO[PACAP/BDNF] neurons stimulation.

(D–F) Stimulation (2 Hz, 30 s) of VMPO[PACAP] (red) or VMPO[BDNF] (blue) neurons induced (D) transient rectal temperature hypothermia. n = 4–7 per group, $F_{7,84}$ (PACAP) = 15.43, p < 0.001; $F_{6,48}$ (BDNF) = 16.16, p < 0.001; (E) increased tail base temperature. n = 7–9 per group, $F_{8,120}$ (PACAP) = 11.43, p < 0.001; $F_{7,84}$ (BDNF) = 14.78, p < 0.001; (F) reduced subcutaneous temperature in the interscapular brown fat deposit. n = 5–10 per group, $F_{10,160}$ (PACAP) = 13.11, p < 0.001; $F_{9,72}$ (BDNF) = 6.70, p < 0.001. All F statistic show two-way RM-ANOVA, group × time interaction.

Values are reported as mean ± SEM. See also Figure S3.

Warm-Sensitive Neurons Control Behavioral Responses to Heat

Behavior is also a critical mechanism of body temperature control. Thermoregulatory behaviors include warm and cold-seeking as well as diverse, species-specific strategies for modulating heat loss, such as nest building in rodents and the use of clothing in humans. These responses to temperature challenge are classic motivated behaviors (Carlisle, 1966; Weiss and Laties, 1961), yet remarkably little is known about their underlying neural substrates (Morrison and Nakamura, 2011; Romanovsky, 2007). Of note, it has been reported that many thermoregulatory behaviors remain intact following pre-optic lesions (Carlisle, 1969; Satinoff and Rutstein, 1970), which has led to the belief that these responses originate from brain structures outside the POA (Satinoff, 1978). However, these lesioning experiments do not preclude a role for the POA in the generation of thermoregulatory behaviors, nor do they clarify the contribution of specific cells and circuits. We therefore investigated the role of VMPO[PACAP/BDNF] neurons in the behavioral response to heat.
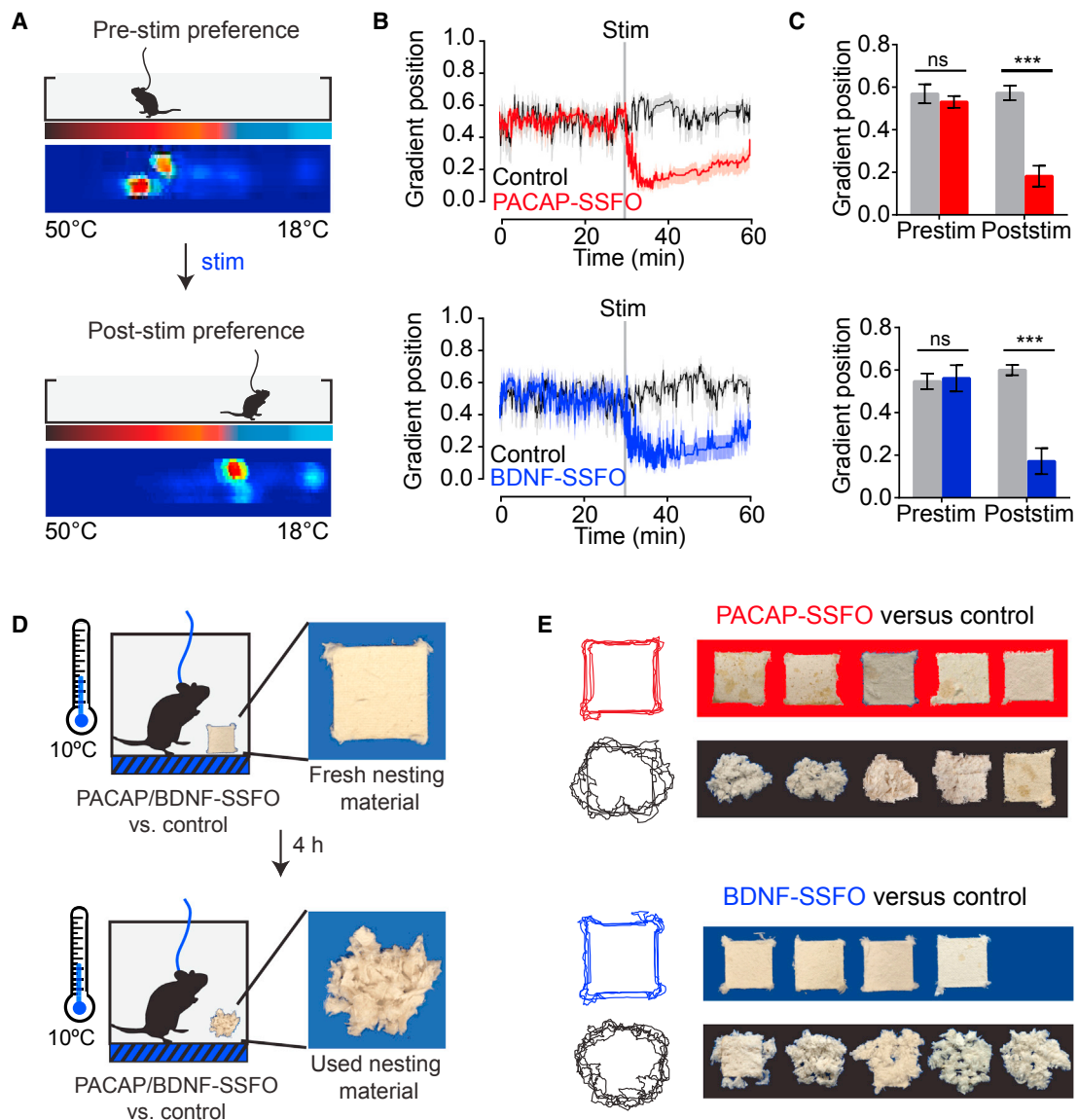
Figure 4. Optogenetic Activation of VMPO$^{PACAP/BDNF}$ Neurons Induces Thermoregulatory Behavior

(A–C) VMPO$^{PACAP/BDNF}$ neuron stimulation alters temperature preference in the thermal gradient. (A) Schematic of thermal gradient assay. Heat map shows cumulative positions of a representative subject on a thermal gradient in the 30-min span before and after light stimulation. (B) Average gradient position (0 = 18°C, 1 = 50°C) during stimulation trials. (C) Median gradient position in the 30-min interval before and after stimulation. n = 7–10 per group. Two-way RM-ANOVA, Interaction, $F_{1,15}$(PACAP) = 37.78, p < 0.001; $F_{1,13}$(BDNF) = 13.90, p = 0.002. post hoc Bonferroni multiple comparisons, ***p < 0.001.

(D–E) POA$^{PACAP/BDNF}$ neuron stimulation suppresses nesting activity. (D) Schematic of nesting activity assay. PACAP-SSFO, BDNF-SSFO, or control subjects were given fresh nesting material in a cool environment (10°C). Light stimulation was applied for 4 hr (10 s of 2 Hz stimulation every 30 min) and condition of nesting material was recorded after. Representative fresh and used nesting material are shown. (E) Photographs (right) of nesting material and a composite of traced outlines are shown after a 4-hr nesting activity assay.

Values are reported as mean ± SEM. See also Figure S4.

We first used a thermal gradient assay that measures temperature preference (Gordon, 1985). Mice were allowed to explore a linear track that varied in temperature across its length (18°C to 50°C; Figure 4A). At baseline, control and SSFO-expressing animals reliably selected 30°C –32°C (Figures 4B and 4C), which approximates thermoneutrality. Upon brief photostimulation, SSFO-expressing animals spontaneously moved to colder tem-

peratures (Figures 4B and 4C, red and blue). This evoked change in temperature preference was rapid, substantial in magnitude (ΔT = −13.6°C and −14.2°C for VMPO^{PACAP} and VMPO^{BDNF} stimulation, respectively), and completely absent from similarly stimulated control mice (Figures 4B and 4C, black). Following this initial response, SSFO-expressing mice gradually migrated back to warmer temperatures over the course of the 30-min trial,
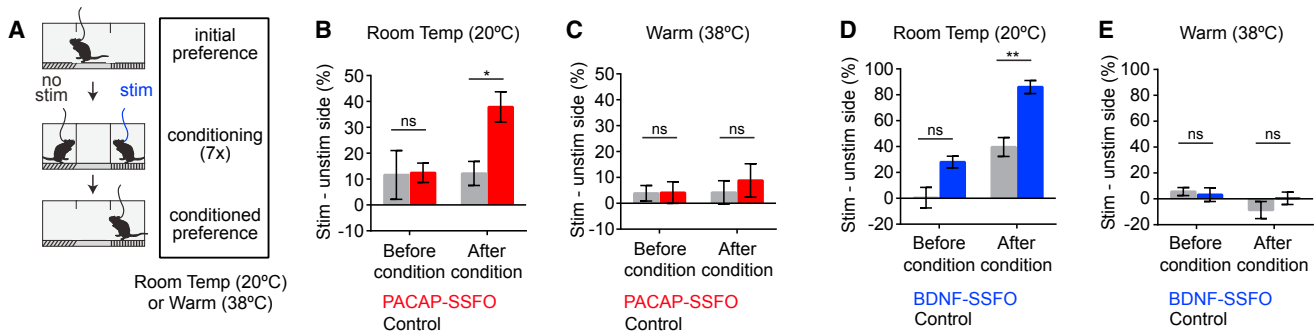
Figure 5. Optogenetic Activation of VMPO$^{PACAP/BDNF}$ Neurons Conditions Place Preference at Cool, but Not at Warm, Ambient Temperatures

(A) Scheme of conditioned place preference test.

(B–E) Difference between proportion of time spent in the stimulation-paired chamber and unpaired chamber for either PACAP-SSFO (B and C) or BDNF-SSFO (D and E) mice at 20°C (B and D) or 38°C (C and E). 20°C: two-way RM-ANOVA, $F_{1,6}$(PACAP, Interaction) = 7.03, p < 0.05; $F_{1,8}$(BDNF, Group) = 18.62, p = 0.002; $F_{1,8}$(BDNF, Conditioning) = 29.25, p < 0.001. 38°C: Two-way RM-ANOVA, All factors p > 0.05. n = 3–6. post hoc Bonferroni multiple comparisons, *p < 0.05, **p < 0.01. Values are reported as mean ± SEM.

consistent with the kinetics of SSFO inactivation. Thus, stimulation of VMPO$^{PACAP/BDNF}$ neurons is sufficient to induce dramatic cold-seeking behavior that develops in unison with core hypothermia (Figure 3D), indicating that these neurons activate a coordinated autonomic and behavioral response to heat.

We next investigated whether activation of these neurons could inhibit corresponding cold-defensive behaviors. Treatment of mice with the super-cooling agent icilin induced robust warm-seeking behavior on a thermal gradient (Figure S4A, gray), which was completely prevented by concurrent photostimulation of VMPO$^{PACAP/BDNF}$ neurons (Figure S4A, red). Thus, activation of warm-sensitive neurons can block the behavioral response to cold. To investigate this further, we measured the effect of VMPO$^{PACAP/BDNF}$ neuron stimulation on nest building, a natural cold-defensive behavior in mice (Figure 4D). We found that control mice robustly tore up nesting material when cold-challenged (10°C) but did so at a much slower rate at warm temperatures (37°C, Figure S4B), confirming that the rate of nest-building is inversely proportional to ambient temperature (Gaskill et al., 2013). Photostimulation of VMPO$^{PACAP/BDNF}$ neurons abolished this cold-induced nesting (Figure 4E, red and blue), whereas control animals were unaffected by photostimulation (Figure 4E, black). Thus, VMPO$^{PACAP/BDNF}$ neuron activation can inhibit cold-defensive behaviors, consistent with a specific role for these neurons in promoting heat loss.

Thermoregulatory behaviors are motivated and therefore are mediated at least in part by changes in reward expectation (Carlisle, 1966; Weiss and Laties, 1961). Stimulation of neurons that encode warmth would be predicted to be rewarding when mice are cold, but not when they are hot. To test this prediction, we used a conditioned place preference assay to measure the valence of warm-sensitive VMPO$^{PACAP/BDNF}$ neuron activity. Control and SSFO-expressing animals were conditioned using two chambers that differed in textural and visual cues, one of which was paired with optical stimulation and the other not (Figure 5A). We performed both conditioning and testing at two different temperatures (20°C and 38°C) on separate cohorts of mice (Figure 5A). These two temperatures are cold and hot, respectively, relative to the preferred ambient temperature of a

mouse (~31°C; Figure 4B). After a 2-week conditioning period, SSFO-expressing subjects at 20°C developed a significant preference for the stimulation-paired chamber (Figures 5B and 5D), whereas SSFO-expressing subjects at 38°C showed no such preference (Figures 5C and 5E). Control mice lacking SSFO-expression showed no conditioned preference at any temperature (Figures 5B–5E). Thus, VMPO$^{PACAP/BDNF}$ neuron activation has positive valence specifically at temperatures below thermoneutrality. This finding is consistent with the observation that mice are chronically cold-stressed at room temperature (Karp, 2012) and therefore likely experience as rewarding the artificial warmth produced by VMPO$^{PACAP/BDNF}$ neuron activation (Figures 5B and 5D).

Organization of the Downstream Thermoregulatory Circuit

The sufficiency of VMPO$^{PACAP/BDNF}$ neurons for autonomic and behavioral thermoregulation suggests that their axon projections may delineate critical brain regions for body temperature control. To visualize this circuitry, we performed anterograde tracing by targeting a Cre-dependent AAV expressing synaptophysin-mCherry to VMPO^{PACAP} neurons (Figures 6A and 6B). This revealed dense projections to a number of brain regions involved in autonomic control, including the dorsomedial hypothalamus (DMH), paraventricular hypothalamus (PVH), and ventrolateral periaqueductal gray (vlPAG), as well as structures associated with motivated behaviors, including the bed nucleus of the stria terminalis (BNST), paraventricular thalamus (PVT), and medial habenula (mHb) (Figure 6C). This circuit organization suggests that VMPO$^{PACAP/BDNF}$ neurons may assemble the diverse autonomic and behavioral responses to heat via their anatomically distinct projections.

To begin to dissect this circuitry, we focused on the DMH, which has been strongly implicated in the control of BAT thermogenesis (Dimicco and Zaretsky, 2007). Pioneering studies showed that pharmacologic activation of the DMH increases heat production (Cao et al., 2004; Zaretskaia et al., 2002), whereas silencing of the DMH has the opposite effect (Nakamura et al., 2005). As the DMH is densely innervated by the POA, it has

A   AAV EF1a-DIO-Syn-mCherry

C   VMPO^PACAP neuron projection targets
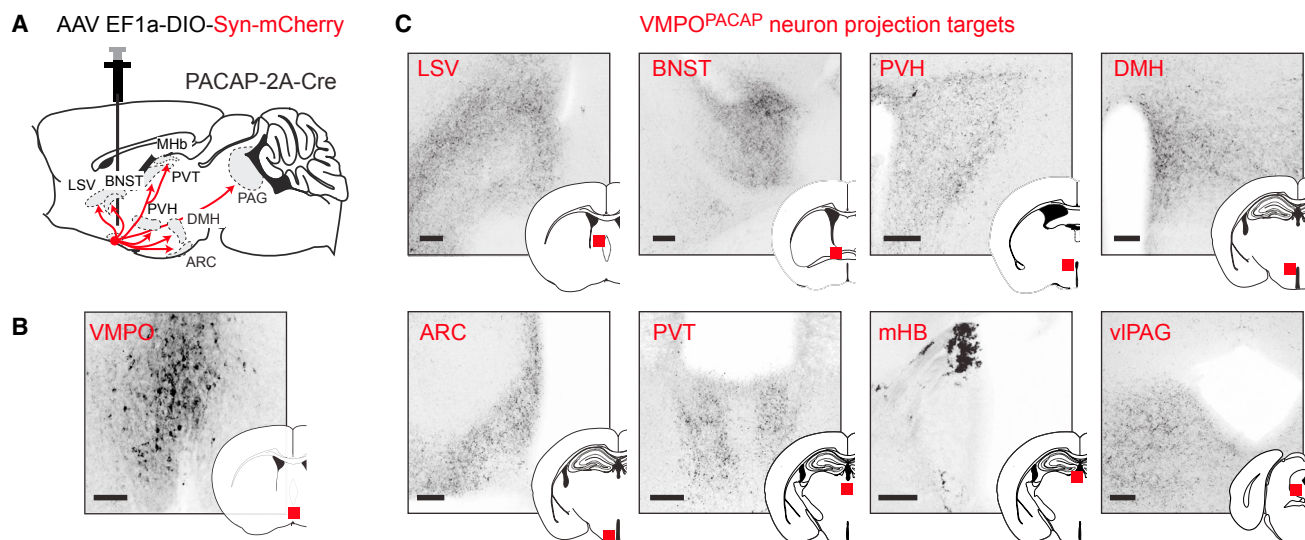
Figure 6. Anterograde Tracing Reveals Downstream Thermoregulatory Circuit

(A) Schematic summarizing strategy for visualizing target structures using Cre-dependent virus expressing a synaptophysin-mCherry fusion protein. Major VMPO^PACAP neuron projection sites are indicated.

(B) Expression of synaptophysin-mCherry (dark) in VMPO^PACAP neurons cell bodies at VMPO injection site.

(C) Expression of synaptophysin-mCherry in VMPO^PACAP neuron terminals at indicated regions (red squares). LSV, ventral portion of lateral septum; BNST, bed nucleus of stria terminalis; DMH, dorsomedial hypothalamus; ARC, arcuate nucleus; PVT, paraventricular thalamus; MHb, medial habenula; PVH, paraventricular hypothalamus; vlPAG, ventrolateral periaqueductal gray. Scale bars, 100 μm. Values are reported as mean ± SEM.

been proposed that warm-sensitive neurons inhibit thermogenesis via a GABAergic POA → DMH projection (Kataoka et al., 2014; Morrison et al., 2014; Nakamura et al., 2005), although direct evidence is lacking. We therefore investigated whether warm-sensitive VMPO^PACAP/BDNF neurons may be the source of this inhibitory projection.

We first confirmed that optogenetic or chemogenetic stimulation of DMH glutamatergic neurons strongly activated BAT thermogenesis, as predicted by current models (Figures S5A–S5F). We then neurochemically characterized the warm-sensitive inputs into this structure by injecting a retrograde HSV expressing a Cre-dependent reporter into the DMH of BDNF-2A-Cre mice (Figure 7A). Co-localization between these retrogradely labeled cells and a GAD2 reporter revealed that more than 90% of VMPO^BDNF neurons that innervate the DMH are GABAergic, indicating a predominantly inhibitory projection (Figure 7B). For comparison, this was somewhat higher than the percentage of GABAergic neurons within the VMPO^BDNF population as a whole (69% ± 1%) or among all VMPO cells showing warm induced pS6 (83% ± 1%).

To test the thermoregulatory function of this projection, we injected a Cre-dependent AAV vector expressing channelrhodopsin (hChR2(H134R), not SSFO) into the VMPO of PACAP-2A-Cre mice and implanted an optical fiber above the DMH (Figure 7C). Optical stimulation of VMPO^PACAP terminals in the DMH progressively inhibited BAT thermogenesis (Figures 7D and 7E, red), whereas stimulation of control animals yielded no response (Figures 7D and 7E, black). This inhibition of BAT thermogenesis was potent, as it was sufficient to block the response to cold-challenge (Figure S5G). It was also spe-

cific, as DMH terminal stimulation had no effect on tail vasodilation (Figure 7F) or behavioral thermoregulation in a gradient assay (Figure 7G). Thus, VMPO^BDNF/PACAP neurons supply a warm-sensitive, GABAergic projection to the DMH that selectively inhibits BAT thermogenesis relative to other thermoregulatory effectors. This shows that the diverse heat-defensive responses of VMPO^BDNF/PACAP neurons can be dissociated, at least in part, through their anatomically segregated axon projections, and prioritizes further investigation of these efferent pathways as a means to elucidate the functional organization of the thermoregulatory circuit.

DISCUSSION

The preoptic hypothalamus has long been recognized as a critical structure for the regulation of body temperature (Clark et al., 1939; Magoun et al., 1938; Teague and Ranson, 1936), yet the identity of the key cell types has remained unclear, hindering efforts to define the neural mechanisms underlying thermoregulation. Here, we have used an unbiased RNA sequencing approach to identify a molecularly defined population of preoptic neurons that are selectively activated in vivo by environmental warmth (Figures 1 and 2), and, in turn, trigger a diverse repertoire of autonomic and behavioral thermoregulatory responses (Figures 3, 4, 5, 6, and 7). This reveals that a single population of warm-activated cells is sufficient to orchestrate the complex homeostatic response to heat. Molecular identification of these thermoregulatory command neurons provides genetic access to core elements of the neural circuit that regulates body temperature in mammals.
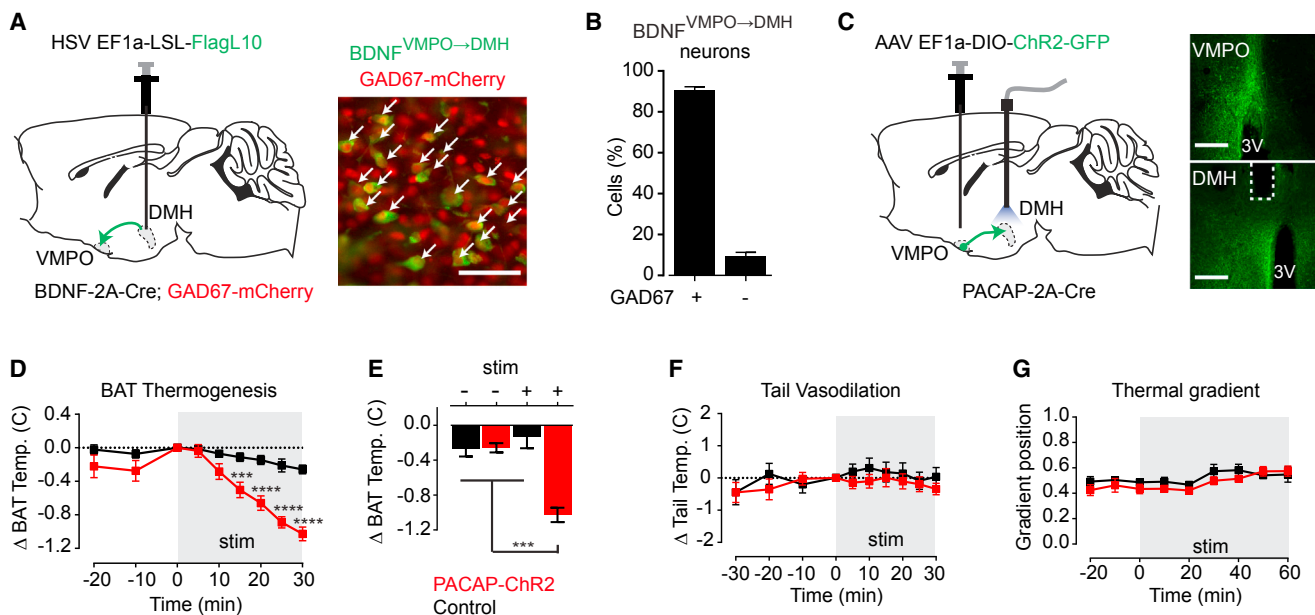
Figure 7. VMPO$^{PACAP/BDNF}$ Neurons Inhibit Brown Fat Thermogenesis via a GABAergic Projection to the DMH

(A) Schematic and representative image of retrograde-labeling of BDNF$^{POA \rightarrow DMH}$ neurons (green) and costaining for nuclear localized GAD67-mCherry (red). Scale bar, 50 μm.

(B) Bar graph quantifies percentage of BDNF$^{VMPO \rightarrow DMH}$ neurons that were GAD67 positive. n = 3.

(C–G) DMH-projection site-specific stimulation. Red, PACAP-ChR2 subjects; black, control subjects. Schematic and images. (C) Expression of hChR2(H134R)-GFP (green) in cell bodies at VMPO injection site and axon terminals at DMH. White dotted line indicate optic fiber placement. Scale bar, 400 μm. (D and E) Interscapular brown fat temperature decreases upon light stimulation in PACAP-ChR2 subjects. (10-ms light pulse at 5 Hz in 1 s ON/1 s OFF duty cycle). n = 8–11 per group. (D) Time course shows change in BAT temperature relative to start of stimulation period shown in gray. Two-way RM-ANOVA, $F_{8,136}$(Group × Time) = 9.154, p < 0.001. (E) Mean brown fat temperature changes after 30 min in the absence or presence of stimulation. Two-way ANOVA, $F_{1,34}$(Group × Stimulation) = 26.04, p < 0.0001. (F) No effects observed on tail vasodilation. Change in tail temperature relative to start of stimulation period shown in gray. n = 11 per group. Two-way RM-ANOVA, All factors, p > 0.05. (G) No effect on preferred temperature as shown by the mean thermal gradient position in 10-min intervals. Stimulation period shown in gray. n = 7 per group. Two-way RM-ANOVA, Interaction and Group factors, p > 0.05. Post hoc Bonferroni multiple comparisons, ***p < 0.001. Values are reported as mean ± SEM. See also Figure S5.

Warm-Sensitive Neurons Are Regulated by Thermal Signals from the Periphery

Local heating of the POA can induce dramatic thermoregulatory responses (Magoun et al., 1938) and a subset of preoptic neurons are directly activated by heat (Nakayama et al., 1961). These observations have led to a textbook model that emphasizes the role of intrinsically thermosensitive neurons within the POA in monitoring the local temperature of the brain and then enacting homeostatic responses (Galizia and Lledo, 2013). However, a complication for this model has been the observation that environmental warm or cold exposure does not alter the temperature of the hypothalamus in a consistent way (Bratincsák and Palkovits, 2005; Forster and Ferguson, 1952; Hammel, 1968; Hellstrom and Hammel, 1967; Morrison and Nakamura, 2011; Nakamura and Morrison, 2007, 2008; Sakurada et al., 1993). Moreover, it is unclear whether preoptic neurons are uniquely thermosensitive compared to neurons from other brain regions (Hellon, 1986). Thus, the importance of local preoptic temperature sensing in the control of body temperature has remained a matter of debate.

The POA also receives abundant input from ascending neural pathways that convey thermal signals from the skin and viscera (Geerling et al., 2016; Nakamura and Morrison, 2007, 2008,

2010). In our experiments, VMPO$^{BDNF/PACAP}$ neurons were activated by environmental warmth within seconds (Figure 2I), which almost certainly reflects activation of cutaneous thermoreceptors rather than much slower changes in intracranial temperature. Consistent with this, we found that peripheral injection of capsaicin rapidly activated VMPO$^{BDNF/PACAP}$ neurons, implying a role for TRPV1$^+$ sensory fibers. In contrast, we found no evidence that VMPO$^{BDNF/PACAP}$ neurons were more intrinsically thermosensitive than neighboring cells when we performed whole-cell patch clamp recordings from acute brain slices (Figures S2L and S2M). Thus, our data are most consistent with a model in which VMPO$^{BDNF/PACAP}$ neurons activate thermoregulatory effectors in response to ascending signals from peripheral sensory neurons, although this does rule out an additional role for local thermosensing in other contexts. The availability of a genetic marker for these cells should enable targeted experiments that investigate the mechanisms for their thermosensitivity in response to different types of temperature challenge.

Warm-Sensitive Neurons Are Narrowly Tuned to Innocuous Warmth

The sensitivity of VMPO$^{BDNF/PACAP}$ neurons to environmental temperature was narrowly tuned to the range of innocuous

warmth (~31°C–40°C), with no detectable response to cold challenge or treatment with the super-cooling agent icilin (Figure 2). This striking selectivity suggests a "labelled lines" model for the thermoregulatory circuit, in which the segregated pathways of warm and cold sensory information that are found in the periphery are preserved at the level of the command neurons in the POA. Consistent with this possibility, we found that cold- and warm-challenge induced pS6 in distinct populations of preoptic neurons (Figures S1D and S1E). This anatomic segregation is reminiscent of the distinct populations of warm- and cold-activated neurons that have been described in the parabrachial nucleus, a brainstem relay for ascending thermal information that projects to the POA (Geerling et al., 2016; Nakamura and Morrison, 2008, 2010). One implication of these findings is that there should exist an as-yet-unidentified population of cold-sensitive neurons in the POA that receives thermal signals originating from cold-activated sensory fibers. Genetic identification of these cells and elucidation of their interactions with warm-sensitive VMPO$^{BDNF/PACAP}$ neurons will be an important area for future investigation.

Warm-Sensitive Neurons Coordinate Autonomic and Behavioral Responses to Heat

A remarkable property of VMPO$^{BDNF/PACAP}$ neurons is their ability to simultaneously induce behavioral and autonomic responses to heat: that is, activation of these neurons causes mice to intensely seek cold (Figure 4B) at the same time that their core body temperature plummets (Figure 3D). This striking coordination of autonomic and behavioral thermoregulation following activation of a single cell type is consistent with classical models that posited the existence of a central controller for body temperature in the brain (Hammel, 1968), although it does not rule out additional layers of regulation.

One important implication of this convergent regulation is that the axon projections of VMPO$^{BDNF/PACAP}$ neurons should reveal the identity of the effector brain regions for thermoregulation, and we have shown that several brain structures implicated in the autonomic control of body temperature are densely innervated by VMPO$^{BDNF/PACAP}$ neurons (Figure 6). Compared to these autonomic responses, much less is known about the neural substrates for behavioral thermoregulation, a fundamental motivated behavior that encompasses everything from nest building in rodents to the use of air conditioning in humans. The fact that VMPO$^{BDNF/PACAP}$ neurons project to a number of structures associated with reward and reinforcement (Figure 6C) prioritizes investigation of these brain regions for their role in encoding this fundamental connection between temperature and motivation.

Warm-Sensitive Neuron Projections Delineate Convergence Points for Homeostatic Integration

We have focused here on the role of warm-sensitive VMPO$^{BDNF/PACAP}$ neurons in coordinating the response to environmental temperature. However, body temperature is also dynamically modulated by input from other homeostatic systems, as reflected in the thermoregulatory responses that occur following changes in sleep, circadian rhythms, immune status, and energy and fluid balance (Morrison and Nakamura, 2011). How and where

in the brain these processes are integrated, so that conflicts between competing homeostatic needs can be resolved, remains unknown. Comparison of the axon projections of warm-sensitive VMPO$^{BDNF/PACAP}$ neurons with those of analogous neurons that control hunger (Broberger et al., 1998) and thirst (McKinley, 2003) reveals innervation of many common second order structures, including the PVH, DMH, BNST, PVT, and PAG (Figure 6). It is possible that these second order structures represent convergence points where the competing needs of the body are harmonized. The molecular identification of dedicated warm-sensitive neurons provides a genetic means to begin to investigate these fundamental interconnections between homeostatic systems.

STAR★METHODS

Detailed methods are provided in the online version of this paper and include the following:

- KEY RESOURCES TABLE
- CONTACT FOR REAGENT AND RESOURCE SHARING
- EXPERIMENTAL MODEL AND SUBJECT DETAILS
- METHOD DETAILS
  - Generation of BDNF-2A-Cre Mice
  - Stereotactic Viral Injection and Photometry/Optogenetic Fiber Implantation
  - Temperature Challenges
  - GFP-Reporter Labeling and Cell Counts
  - PhosphoTRAP
  - TRAP
  - RNA Sequencing Analysis
  - Fiber Photometry Recording
  - Fiber Photometry Analysis
  - Optogenetic Stimulation
  - Brown Fat, Tail, and Core Temperature Measurement
  - Thermal Gradient Assay
  - Nesting Behavior Assay
  - Conditioned Place Preference Test
  - Acute Hypothalamic Slice Preparation and Slice Electrophysiology
  - Anterograde-Tracing
  - Retrograde-Labeling
  - Chemogenetic Stimulation
  - Immunohistochemistry
  - In Situ Hybridization
- QUANTIFICATION AND STATISTICAL ANALYSIS
- DATA AND SOFTWARE AVAILABILITY
  - Data Resources

SUPPLEMENTAL INFORMATION

Supplemental Information includes five figures and one table and can be found with this article online at http://dx.doi.org/10.1016/j.cell.2016.08.028.

An audio PaperClip is available at http://dx.doi.org/10.1016/j.cell.2016.08.028#mmc2.

AUTHOR CONTRIBUTIONS

REFERENCES

Boulant, J.A., and Hardy, J.D. (1974). The effect of spinal and skin temperatures on the firing rate and thermosensitivity of preoptic neurones. J. Physiol. 240, 639–660.

Bratincsák, A., and Palkovits, M. (2005). Evidence that peripheral rather than intracranial thermal signals induce thermoregulation. Neuroscience 135, 525–532.

Broberger, C., Johansen, J., Johansson, C., Schalling, M., and Hökfelt, T. (1998). The neuropeptide Y/agouti gene-related protein (AGRP) brain circuitry in normal, anorectic, and monosodium glutamate-treated mice. Proc. Natl. Acad. Sci. USA 95, 15043–15048.

Cao, W.H., Fan, W., and Morrison, S.F. (2004). Medullary pathways mediating specific sympathetic responses to activation of dorsomedial hypothalamus. Neuroscience 126, 229–240.

Carlisle, H.J. (1966). Behavioural significance of hypothalamic temperature-sensitive cells. Nature 209, 1324–1325.

Carlisle, H.J. (1969). Effect of preoptic and anterior hypothalamic lesions on behavioral thermoregulation in the cold. J. Comp. Physiol. Psychol. 69, 391–402.

Caterina, M.J., Schumacher, M.A., Tominaga, M., Rosen, T.A., Levine, J.D., and Julius, D. (1997). The capsaicin receptor: a heat-activated ion channel in the pain pathway. Nature 389, 816–824.

Chen, Y., Lin, Y.C., Kuo, T.W., and Knight, Z.A. (2015). Sensory detection of food rapidly modulates arcuate feeding circuits. Cell 160, 829–841.

Clark, G., Magoun, H.W., and Ranson, S.W. (1939). Hypothalamic regulation of body temperature. J. Neurophysiol. 2, 61–80.

Crane, J.D., Mottillo, E.P., Farncombe, T.H., Morrison, K.M., and Steinberg, G.R. (2014). A standardized infrared imaging technique that specifically detects UCP1-mediated thermogenesis in vivo. Mol. Metab. 3, 490–494.

Dimicco, J.A., and Zaretsky, D.V. (2007). The dorsomedial hypothalamus: a new player in thermoregulation. Am. J. Physiol. Regul. Integr. Comp. Physiol. 292, R47–R63.

Forster, R.E., and Ferguson, T.B. (1952). Relationship between hypothalamic temperature and thermo-regulatory effectors in unanesthetized cat. Am. J. Physiol. 169, 255–269.

Galizia, C.G., and Lledo, P.-M. (2013). Neurosciences: From Molecule to Behavior: A University Textbook (Heidelberg, New York: Springer Spektrum).

Garami, A., Pakai, E., Oliveira, D.L., Steiner, A.A., Wanner, S.P., Almeida, M.C., Lesnikov, V.A., Gavva, N.R., and Romanovsky, A.A. (2011). Thermoregulatory phenotype of the Trpv1 knockout mouse: thermoeffector dysbalance with hyperkinesis. J. Neurosci. 31, 1721–1733.

Gaskill, B.N., Karas, A.Z., Garner, J.P., and Pritchett-Corning, K.R. (2013). Nest building as an indicator of health and welfare in laboratory mice. J. Vis. Exp. Dec 24, 51012.

Geerling, J.C., Kim, M., Mahoney, C.E., Abbott, S.B., Agostinelli, L.J., Garfield, A.S., Krashes, M.J., Lowell, B.B., and Scammell, T.E. (2016). Genetic identity of thermosensory relay neurons in the lateral parabrachial nucleus. Am. J. Physiol. Regul. Integr. Comp. Physiol. 310, R41–R54.

Gordon, C.J. (1985). Relationship between autonomic and behavioral thermoregulation in the mouse. Physiol. Behav. 34, 687–690.

Gunaydin, L.A., Grosenick, L., Finkelstein, J.C., Kauvar, I.V., Fenno, L.E., Adhikari, A., Lammel, S., Mirzabekov, J.J., Airan, R.D., Zalocusky, K.A., et al. (2014). Natural neural projection dynamics underlying social behavior. Cell 157, 1535–1551.

Hammel, H.T. (1968). Regulation of internal body temperature. Annu. Rev. Physiol. 30, 641–710.

Hardy, J.D., Hellon, R.F., and Sutherland, K. (1964). Temperature-sensitive neurones in the dog's hypothalamus. J. Physiol. 175, 242–253.

Harris, J.A., Hirokawa, K.E., Sorensen, S.A., Gu, H., Mills, M., Ng, L.L., Bohn, P., Mortrud, M., Ouellette, B., Kidney, J., et al. (2014). Anatomical characterization of Cre driver mice for neural circuit mapping and manipulation. Front. Neural Circuits 8, 76.

Heiman, M., Kulicke, R., Fenster, R.J., Greengard, P., and Heintz, N. (2014). Cell type-specific mRNA purification by translating ribosome affinity purification (TRAP). Nat. Protoc. 9, 1282–1291.

Hellon, R.F. (1986). Are single-unit recordings useful in understanding thermoregulation? Yale J. Biol. Med. 59, 197–203.

Hellstrom, B., and Hammel, H.T. (1967). Some characteristics of temperature regulation in the unanesthetized dog. Am. J. Physiol. 213, 547–556.

Karp, C.L. (2012). Unstressing intemperate models: how cold stress undermines mouse modeling. J. Exp. Med. 209, 1069–1074.

Kataoka, N., Hioki, H., Kaneko, T., and Nakamura, K. (2014). Psychological stress activates a dorsomedial hypothalamus-medullary raphe circuit driving brown adipose tissue thermogenesis and hyperthermia. Cell Metab. 20, 346–358.

Knight, Z.A., Tan, K., Birsoy, K., Schmidt, S., Garrison, J.L., Wysocki, R.W., Emiliano, A., Ekstrand, M.I., and Friedman, J.M. (2012). Molecular profiling of activated neurons by phosphorylated ribosome capture. Cell 151, 1126–1137.

Lee, H., Kim, D.W., Remedios, R., Anthony, T.E., Chang, A., Madisen, L., Zeng, H., and Anderson, D.J. (2014). Scalable control of mounting and attack by Esr1+ neurons in the ventromedial hypothalamus. Nature 509, 627–632.

Magoun, H.W., Harrison, F., Brobek, J.R., and Ranson, S.W. (1938). Activation of heat loss mechanisms by local heating of the brain. J. Neurophysiol. 1, 101–114.

McAllen, R.M., Tanaka, M., Ootsuka, Y., and McKinley, M.J. (2010). Multiple thermoregulatory effectors with independent central controls. Eur. J. Appl. Physiol. 109, 27–33.

McKemy, D.D., Neuhausser, W.M., and Julius, D. (2002). Identification of a cold receptor reveals a general role for TRP channels in thermosensation. Nature 416, 52–58.

McKinley, M.J. (2003). The Sensory Circumventricular Organs of the Mammalian Brain: Subfornical Organ, OVLT and Area Postrema (Berlin, New York: Springer-Verlag).

McKinley, M.J., Yao, S.T., Uschakov, A., McAllen, R.M., Rundgren, M., and Martelli, D. (2015). The median preoptic nucleus: front and centre for the regulation of body fluid, sodium, temperature, sleep and cardiovascular homeostasis. Acta Physiol. (Oxf.) 214, 8–32.

Morrison, S.F., and Nakamura, K. (2011). Central neural pathways for thermoregulation. Front. Biosci. (Landmark Ed.) 16, 74–104.

Morrison, S.F., Madden, C.J., and Tupone, D. (2014). Central neural regulation of brown adipose tissue thermogenesis and energy expenditure. Cell Metab. *19*, 741–756.

Nagashima, K., Nakai, S., Tanaka, M., and Kanosue, K. (2000). Neuronal circuitries involved in thermoregulation. Auton. Neurosci. *85*, 18–25.

Nakamura, K., and Morrison, S.F. (2007). Central efferent pathways mediating skin cooling-evoked sympathetic thermogenesis in brown adipose tissue. Am. J. Physiol. Regul. Integr. Comp. Physiol. *292*, R127–R136.

Nakamura, K., and Morrison, S.F. (2008). A thermosensory pathway that controls body temperature. Nat. Neurosci. *11*, 62–71.

Nakamura, K., and Morrison, S.F. (2010). A thermosensory pathway mediating heat-defense responses. Proc. Natl. Acad. Sci. USA *107*, 8848–8853.

Nakamura, Y., Nakamura, K., Matsumura, K., Kobayashi, S., Kaneko, T., and Morrison, S.F. (2005). Direct pyrogenic input from prostaglandin EP3 receptor-expressing preoptic neurons to the dorsomedial hypothalamus. Eur. J. Neurosci. *22*, 3137–3146.

Nakayama, T., Eisenman, J.S., and Hardy, J.D. (1961). Single unit activity of anterior hypothalamus during local heating. Science *134*, 560–561.

Romanovsky, A.A. (2007). Thermoregulation: some concepts have changed. Functional architecture of the thermoregulatory system. Am. J. Physiol. Regul. Integr. Comp. Physiol. *292*, R37–R46.

Sakurada, S., Shido, O., Fujikake, K., and Nagasaka, T. (1993). Relationship between body core and peripheral temperatures at the onset of thermoregulatory responses in rats. Jpn. J. Physiol. *43*, 659–667.

Satinoff, E. (1978). Neural organization and evolution of thermal regulation in mammals. Science *201*, 16–22.

Satinoff, E., and Rutstein, J. (1970). Behavioral thermoregulation in rats with anterior hypothalamic lesions. J. Comp. Physiol. Psychol. *71*, 77–82.

Scammell, T.E., Price, K.J., and Sagar, S.M. (1993). Hyperthermia induces c-fos expression in the preoptic area. Brain Res. *618*, 303–307.

Scott, N., Prigge, M., Yizhar, O., and Kimchi, T. (2015). A sexually dimorphic hypothalamic circuit controls maternal care and oxytocin secretion. Nature *525*, 519–522.

Stujenske, J.M., Spellman, T., and Gordon, J.A. (2015). Modeling the spatio-temporal dynamics of light and heat propagation for in vivo optogenetics. Cell Rep. *12*, 525–534.

Suter, K.J., Song, W.J., Sampson, T.L., Wuarin, J.P., Saunders, J.T., Dudek, F.E., and Moenter, S.M. (2000). Genetic targeting of green fluorescent protein to gonadotropin-releasing hormone neurons: characterization of whole-cell electrophysiological properties and morphology. Endocrinology *141*, 412–419.

Teague, R.S., and Ranson, S.W. (1936). The role of the anterior hypothalamus in temperature regulation. Am. J. Physiol. *117*, 562–570.

Weiss, B., and Laties, V.G. (1961). Behavioral thermoregulation. Science *133*, 1338–1344.

Wu, Z., Autry, A.E., Bergan, J.F., Watabe-Uchida, M., and Dulac, C.G. (2014). Galanin neurons in the medial preoptic area govern parental behaviour. Nature *509*, 325–330.

Yizhar, O., Fenno, L.E., Prigge, M., Schneider, F., Davidson, T.J., O'Shea, D.J., Sohal, V.S., Goshen, I., Finkelstein, J., Paz, J.T., et al. (2011). Neocortical excitation/inhibition balance in information processing and social dysfunction. Nature *477*, 171–178.

Yoshida, K., Konishi, M., Nagashima, K., Saper, C.B., and Kanosue, K. (2005). Fos activation in hypothalamic neurons during cold or warm exposure: projections to periaqueductal gray matter. Neuroscience *133*, 1039–1046.

Zaretskaia, M.V., Zaretsky, D.V., Shekhar, A., and DiMicco, J.A. (2002). Chemical stimulation of the dorsomedial hypothalamus evokes non-shivering thermogenesis in anesthetized rats. Brain Res. *928*, 113–125.

Zhang, Y., Kerman, I.A., Laque, A., Nguyen, P., Faouzi, M., Louis, G.W., Jones, J.C., Rhodes, C., and Münzberg, H. (2011). Leptin-receptor-expressing neurons in the dorsomedial hypothalamus and median preoptic area regulate sympathetic brown adipose tissue circuits. J. Neurosci. *31*, 1873–1884.

STAR★METHODS

KEY RESOURCES TABLE

REAGENT or RESOURCE	SOURCE	IDENTIFIER
Antibodies		
Rabbit Polyclonal anti-Phospho-Ribosomal protein S6 pSer244/pSer247	Invitrogen	Cat# 44-923G RRID:AB_2533798
Mouse monoclonal anti-GFP	Memorial-Sloan Kettering Monoclonal Antibody Facility	Htz-GFP-19F7 Htz-GFP-19C8
Chicken polyclonal anti-GFP	Abcam	Cat# ab13970 RRID:AB_300798
Rat monoclonal anti-RFP	Chromotek	Cat# rfp-antibody-5f8 RRID:AB_2336064
Mouse monoclonal anti-galactosidase Beta	Promega	Cat# Z378A RRID:AB_2313752
Mouse monoclonal anti-NeuN	Millipore	Millipore Cat# MAB377, RRID:AB_2298772
Chemicals, Peptides, and Recombinant Proteins		
Icilin	Sigma-Aldrich	Cat# I9532; CAS: 36945-98-9
Capsaicin	Calbiochem EMD Millipore	Cat# 211275; CAS: 404-86-4
Clozapine-N-oxide	Tocris Bioscience	Cat# 4936; CAS: 34233-69-7
Critical Commercial Assays		
Ovation RNA-Seq System V2	Nugen	Cat#7102-08
Ovation Ultralow DR Multiplex system	Nugen	Cat#0330
RNAscope Manual Fluorescent Multiplex kit	Advanced Cell Diagnostics	Cat#320293/320513
Deposited Data		
PhosphoTRAP RNA-Seq raw and analyzed data	This paper	GEO: GSE80121
TRAP-Seq RNA-Seq raw and analyzed data	This paper	GEO: GSE80120
Experimental Models: Organisms/Strains		
Mouse: PACAP-2A-Cre/Adcyap1-2A-Cre	Allen Institute for Brain Science	NA
Mouse: BDNF-2A-Cre	This paper	NA
Mouse: Gal-Cre: B6.FVB(Cg)-Tg(Gal-cre)K187Gsat/Mmucd	Mutant Mouse Resource and Research Centers	031060-UCD
Mouse: Vglut2-IRES-Cre: $Slc17a6^{tm2(cre)Lowl}$	The Jackson Laboratory	016963
Mouse: Gad2-2A-nls-mcherry: B6;129S-$Gad2^{tm1.1Ksvo}$/J	The Jackson Laboratory	023140
Mouse: Nos1-IRES-Cre: B6.129-$Nos1^{tm1(cre)Mgmj}$/J	The Jackson Laboratory	017526
Mouse: BDNF-LSL-LacZ: B6.129S2(Cg)-$Bdnf^{tm1Krj}$/J	The Jackson Laboratory	021055
Mouse: Rosa26-LSL-GFPL10a: B6.129S4-$Gt(ROSA)26Sor^{tm1(CAG-EGFP/Rpl10a,-birA)Wtp}$/J	The Jackson Laboratory	022367
Recombinant DNA		
AAV2- EF1a-DIO-EGFP-L10a	This Paper (packaged by UNC vector core)	NA
AAV1-CAG-DIO-GCAMP6s	Upenn Vector Core	NA
AAV5- hEF1α -DIO-hChR2(C128S/D156A)-eYFP [SSFO]	UNC Chapel Hill Vector Core	NA
AAV5- EF1a- DIO-hChR2(H134R)-eYFP	UNC Chapel Hill Vector Core	NA
AAV9-hEF1α- DIO-Synaptophysin-mCherry	MIT McGovern Viral Core Facility	NA
HSV-hEF1α-LSL-HAFlagL10a-WPRE-SV40	This paper (packaged by MIT McGovern Viral Core)	NA
AAV2-EF1a-DIO-hM3Dq-mcherry	UNC Chapel Hill Vector Core	NA
Sequence-Based Reagents		
EGFP In situ hybridization probe	Advanced Cell Diagnostics	400281-C3
mm-BDNF In situ hybridization probe	Advanced Cell Diagnostics	424821

(Continued on next page)

Continued

REAGENT or RESOURCE	SOURCE	IDENTIFIER
BDNF sgRNA sequence: CCATTAAAAGGGGAAGATAGG TTTAAGAGCTATGCTGGAAACAGCATAGCAAGTTTAAA TAAGGCTAGTCCGTTATCAACTTGAAAAAGTGGCACC GAGTCGGTGCTTTTTTT	This Paper	NA
BDNF-2A-Cre genotyping primers: Fwd: TCAATACCGGAGATCATGCAAGC Rev: CTGCTGCCATGCATAAAACATT	This Paper	NA
Software and Algorithms		
ArrayStar Version 11.0	DNASTAR Inc.	NA
pClamp 10.5	Molecular Devices	NA
GraphPad Prism 7.0	GraphPad	NA

CONTACT FOR REAGENT AND RESOURCE SHARING

Further information and requests for reagents may be directed to, and will be fulfilled by the corresponding author Zachary Knight (zachary.knight@ucsf.edu).

EXPERIMENTAL MODEL AND SUBJECT DETAILS

All animals were maintained on a 12 hr light/dark cycle and given ad libitum access to chow (PicoLab Rodent Diet 5053) and water. Wild-type mice were obtained from Jackson Laboratories (Bar Harbor, ME). Genotypes and sources of transgenic animals used are listed in the Key Resources Table. All transgenic mice used in these studies were on the C57Bl/6J background, except BDNF-2A-Cre mice that were maintained on a mixed FVB/C57Bl/6J background. Mice were at least six weeks old at the time of surgery. Unless otherwise stated, all studies employed a mixture of male and female mice and no differences between sexes were observed. All procedures were conducted during the light cycle. All experimental protocols were approved by the University of California, San Francisco IACUC following the National Institutes of Health guidelines for the Care and Use of Laboratory Animals.

METHOD DETAILS

Generation of BDNF-2A-Cre Mice

The bicistronic BDNF-2A-Cre allele was generated by homologous recombination at the endogenous BDNF locus, aided by targeted CRISPR endonuclease activity. Briefly, homology regions were captured into a plasmid from BAC containing the BDNF locus by recombineering. The T2A-Cre sequence was inserted just before the endogenous STOP codon. The final targeting vector contained 2.5 kb homology arms and was verified by restriction digest and sequencing. To generate site-specific double stranded breaks using CRISPR, a sgRNA sequence was selected such that the guide sequence would be separated from the PAM site in the genomic DNA by the 2A-Cre insertion. This ensured that the targeting vector and recombined BDNF allele were protected from Cas9 nuclease activity. Super-ovulated female FVB/N mice were mated to FVB/N stud males, and fertilized zygotes were collected from oviducts. Cas9 protein (100 ng/μL), sgRNA (50 ng/μL) and targeting vector DNA (20 ng/μL) were mixed and injected into pronucleus of fertilized zygotes. Injected zygotes were implanted into oviducts of pseudopregnant CD1 female mice. Out of 15 pups genotyped, four were positive for the knockin, and three of these also contained the targeting vector inserted randomly as a transgene. The transgene was bred out by backcrossing to C57Bl/6J, and two of these independent knockin lines were crossed to reporter mice. Reporter expression patterns were identical to each other and to the endogenous BDNF expression in the brain. All BDNF-2A-Cre mice used here were maintained on mixed FVB/C57Bl/6J background. Founder pups and offspine were genotyped for the presence of the knockin allele by PCR (expected size 2731 bp). SgRNA sequence and genotyping primer sequences are listed in the Key Resources Table.

Stereotactic Viral Injection and Photometry/Optogenetic Fiber Implantation

Animals were anesthetized with 2% isoflurane and placed in a stereotaxic head frame. Ophthalmic ointment was applied to the eyes and a subcutaneous injection of carprofen (10 mg/kg) was given to each mouse prior to surgery and one day after. The scalp was shaved, local anesthetic applied (lidocaine, 0.5%), and then incised through the midline. A craniotomy was made using a dental drill (0.5 mm). A Nanofil Hamilton syringe (2 μL; WPI, Sarasota, FL) with a 26 gauge beveled metal needle was used to infuse virus. Virus was infused at a rate of 100 nL/min. Following infusion, the needle was kept at the injection site for 10min and then slowly withdrawn. Virus preparations were injected bilaterally at the following coordinates. VMPO: AP +0.50 mm, ML ± 0.30 mm,

DV −5.10 mm relative to bregma; DMH: AP −1.55 mm, ML ± 0.35 mm, DV −5.10 mm. All virus preparations (300 nL) were injected bilaterally.

Separate craniotomies were made for photometry/optogenetic fiber implants if necessary and optogenetic fiber tips were inserted to the following coordinates: VMPO: AP +0.45 mm, ML −0.25 mm, DV −4.60 mm; DMH: AP −1.55 mm, ML ± 0.00 mm, DV −4.60 mm. Photometry fiber implants were inserted to the same coordinates as the viral injections. Cannulas were inserted slowly and secured to the skull using a thin base layer of Vetbond (Santa Cruz Biotechnology, sc-361931) and adhesive dental cement (a-m systems 525000 and 526000). The incision was closed with Vetbond and animals were given a subcutaneous injection of buprenorphine (0.05 mg/kg) prior to recovery over a heat pad. Mice were monitored daily for wound healing, food intake and body weight, and allowed to recover for a minimum of two weeks before the initiation of experiments.

Temperature Challenges

For temperature challenges prior to pS6 IHC or phosphoTRAP experiments, mice were kept in their home cages and cages were placed in large temperature controlled chamber (RIS33SD, Powers Scientific) set at 4°C or 37°C for four hours. For temperature challenges during photometry recording or optogenetic stimulation, a custom temperature chamber (approx. 3 in X 4 in X 3 in) was constructed using Peltier floor plate (TE Tech, CP065) wired to a temperature controller (TE Tech, TC720) and enclosed by Plexiglas chamber walls.

GFP-Reporter Labeling and Cell Counts

To broadly label POA^{BDNF} or POA^{PACAP} neurons with GFP-L10a, custom-made AAV2-EF1a-DIO-EGFP-L10a virus (300 nL) was injected bilaterally into the VMPO of PACAP-2A-Cre or BDNF-2A-Cre mice. Resulting PACAP-GFP or BDNF-GFP subjects were challenged with warm or cold temperatures and used for IHC and costained for phosphorylated S6.

To quantify NeuN and Gad67-mcherry overlap with PACAP/BDNF neurons in the VMPO, 20X Z-stack images taken from 50 μm coronal slices (Bregma +0.4 to +0.5) were taken and number of marker/GFP double positive, or singly positive cells were counted (FIJI). Estimate of total neurons in the POA (1.0 mm X 1.5 mm) at the same coronal section (Bregma +0.4 to +0.5) was obtained by counting number of NeuN positive cells in a 0.5 X 0.5 mm area and multiplying by a factor of 6. Within the VMPO narrowly defined (the medial ventral triangle located at bregma +0.4 to 0.5 mm), 42% ± 3% of neurons are BDNF+. Within the broader POA in the same section (bregma +0.4 to 0.5 mm), 13% ± 1% of neurons are BDNF+

PhosphoTRAP

Detailed protocol and buffer recipes are described previously (Knight et al., 2012). Briefly, mice were rapidly sacrificed by cervical dislocation and brains were removed, rinsed briefly with cold dissection buffer and place in a cold sectioning matrix. 0.5 mm sections were obtained and the anterior hypothalamus was removed under a dissecting microscope. Tissue from 5-8 brains was pooled for each experimental repeat, and a total of three experimental repeats were performed. Pooled tissue was homogenized and clarified by centrifugation. Ribosomes were immunoprecipitated using polyclonal antibody against phosphoS6(244/247) (Invitrogen #44923G) that was previously conjugated to Protein A coated magnetic beads (ThermoFisher Scientific). An aliquot of input RNA taken prior to immunoprecipitation and total immunoprecipitated RNA were then purified using the RNAeasy Micro kit (QIAGEN). All RNA sample quality was checked using RNA PicoChip on a bioanalyzer and only samples with RIN > 8 were used. Amplified cDNA was prepared using Ovation RNA-Seq System V2, and sequencing library was prepared using the Ovation Ultralow DR Multiplex system and sequenced on an Illumina HiSeq2500 platform. Raw and analyzed data deposited at Gene Expression Omnibus (GEO) database (accession number GSE80121).

TRAP

Custom recombinant cre-dependent AAV expressing GFP-tagged ribosomal subunit L10a (AAV2-EF1a-DIO-EGFP-L10a) was cloned and then packaged by UNC vectors core. 300 nL of viral aliquot was injected bilaterally into the VMPO. Animals were sacrificed for immunoprecipitation 2-3 weeks after injection. For TRAP experiments, a nearly identical protocol to phosphoTRAP was used except tagged ribosomes were immunopreciated using anti-EGFP antibody (equal mixture of clones 19C8 and 19F7 from Monoclonal Antibody Core Facility at Memorial Sloan-Kettering cancer center). Cut-offs were applied to remove low expression genes (read count > 0, RPKM > 1 for either input or IP sample). Two experimental repeats were performed for both BDNF-TRAP and PACAP-TRAP, each repeat pools tissue dissected from 6-10 mice. Table S1 list genes selectively enriched VMPO$^{BDNF/PACAP}$ neurons. Only genes in which enrichment was above indicated threshold in all experimental repeats were included. GEO accession number GSE80120.

RNA Sequencing Analysis

RNA-seq reads from all input (IN) and immunoprecipitated (IP) samples were trimmed for adaptor and index sequences and aligned to annotated mRNAs in the mouse genome (UCSC, *Mus musculus* assembly mm9), and read count and RPKM values for each gene was calculated using ArrayStar software (DNAstar). Cut-offs were applied to remove low expression genes (read count > 0, RPKM > 1 for either input or IP sample). For PhosphoTRAP data, p value for each gene was calculated as the paired t test between input and

immunoprecipitated RPKM values from the three experimental repeats. For both PhosphoTRAP and TRAP datasets, enrichment ratio of RPKM values was calculated for each paired sample (IP/IN). Enrichment ratio are expressed on log2 scale.

Fiber Photometry Recording

AAV1-CAG-DIO-GCAMP6s vectors were purchased from the Penn Vector Core and virus (300 nL) was injected bilaterally into VMPO as described above. A rig for performing fiber photometry recordings was previously described (Chen et al., 2015). Briefly, a 473 nm laser diode (Omicron Luxx) was used as the excitation source. This was placed upstream of an optic chopper (Thorlabs MC2000) that was run at 400 Hz and then passed through a GFP excitation filter (Thorlabs MF469-35). This signal was then reflected by a dichroic mirror and coupled through a fiber collimation package (Thorlabs F240FC-A) into a home-made patchcord made with optical fiber (400 μm, 0.48 NA; Thorlabs BFH48-400). This patchcord was then linked to a home-made implant fiber optic (Thorlabs BFH48-400, CF440-10) through ceramic splitting sleeve (Thorlabs ADAF15). Fluorescence output was filtered through a GFP emission filter (Thorlabs MF525-39) and focused by a convex lens (Thorlabs LA1255A) onto a photoreceiver (Newport 2151). The signal was output into a lock-in amplifier (Stanford Research System, SR810) with time constant at 100 ms to allow filtering of noise at higher frequency. Signal was then digitized with LabJack U6-Pro and recorded using software provided by LabJack (http://labjack.com/support/software) with 250 Hz sampling rate.

All animals were allowed to recover after patch cord attachment for at least 30 min.

For temperature challenges, the animal was placed in a small custom-built temperature chamber (approx. 3 in X 4 in X 3 in) was constructed using Peltier floor plate (TE Tech, CP065) and enclosed by Plexiglas chamber walls and lid. This set-up prevents animal escape, but allowed free movement within chamber after attachment. Chamber temperature changes were controlled by an external controller (TE Tech, TC720).

For capsaicin/icilin and non-specific stimulus presentation, experiments were conducted in a fresh empty housing cage. In capsaicin/icilin experiments, drugs were prepared fresh on the day of experiment by dilution in vehicle solution (0.9% sterile saline supplemented with 5% PEG400 and 5% Tween-80) and injected intraperitoneally at a volume (μL) equal to 10X body weight (g) to achieve a final dosage of 2 mg/kg (capsaicin) or 5 mg/kg (icilin). Paired vehicle injection of equal volume was administered 30 min before drug injection. Subsequent capsaicin/icilin responses were normalized to response to vehicle injection (See Fiber Photometry Analysis). Capsaicin and Icilin responses were assayed on separate days. For non-specific stimulus presentation, the following items were sequentially placed into the cage for 30 min each: novel object (wood block), regular chow, a spoonful of peanut butter, novel mouse of the same sex.

To assay responses in MPOA galanin-expressing cells, AAV1-CAG-DIO-GCAMP6s virus was injected unilaterally into the MPOA: AP 0.00 mm, ML $\pm$ 0.50 mm, DV -5.25 mm.

To assay responses in SFO Nos1-expressing cells, AAV1-CAG-DIO-GCAMP6s virus was injected at these coordinates: AP -0.50 mm, ML 0.00 mm, DV -2.75 mm.

For GFP controls, AAV2-EF1a-DIO-EGFP-L10a was injected to the VMPO instead of GCAMP6s expressing virus. Photometry fiber implants were inserted so that tips were placed at the same coordinates as virus injection.

Fiber Photometry Analysis

All data were subjected to the following minimal processing steps in MATLAB. Recorded fluorescence from each continuous experimental trial was normalized to the median fluorescence over the trial, decimate function was applied to reduce sampling rate to 1 Hz, and smoothing was applied using moving average filter with span of five elements. For calculation of ΔF/F in all temperature challenge and non-specific stimulus experiments, baseline F_0 was defined as the average fluorescence at 25°C in the 1000 s interval before start of first temperature change or first stimulus presentation. For rapid temperature transitions (15°C$\rightarrow$ 40°C$\rightarrow$15°C), F_0 was defined as the average fluorescence at 15°C. For capsaicin and icilin injection experiments, F_0 was defined as the average fluorescence in the 1000 s interval following vehicle injection. Animals were sacrificed for IHC after completion of experiments to confirm specificity of viral expression and fiber placement. Subjects that showed no expression of GCAMP6s by IHC were excluded.

Optogenetic Stimulation

AAV stocks AAV5- hEF1α -DIO-hChR2(C128S/D156A)-eYFP [SSFO] and AAV5- EF1a-DIO-hChR2(H134R)-eYFP were purchased from University of North Carolina at Chapel Hill Vector Core and 300 nL of viral aliquot was injected bilaterally into the VMPO or DMH as described above Homemade optical fiber implants (CFLC230-10, FT200EMT, ThorLab) were implanted above the VMPO (SSFO) or DMH (hChR2) as described above. Control group was injected with GFP virus (AAV2-EF1a-DIO-EGFP-L10a) and similarly implanted with optical fiber. During stimulation experiments, implanted cannulated fibers were attached to patch cable using ceramic sleeves (ADAL1-5, Thorlab). Patch cables were in turn connected to 473 nm DPSS laser (BL473T8U-200FC, SLOC). Laser output at end of patch cable were verified at start of experiment. Laser pulse width and frequency was controlled by external microcontroller (Arduino). Laser Output at fiber tip = 10 mW for all experiments unless otherwise indicated and light pulse-width = 10 ms for all stimulation. SSFO stimulation was applied at 2 Hz for 30 s unless otherwise indicated, hChR2 DMH-terminal stimulation was applied at 5Hz with 1 s ON/1 s OFF duty cycle for the indicated duration. Animals were allowed to habituate for an hour before start of experiments. Animals were sacrificed for IHC after completion of experiments to confirm specificity of viral expression and fiber placement.

Some animals showed no expression of eYFP by IHC and were grouped with the rest of the control group for analysis. No differences were observed between GFP and IHC-negative groups.

Brown Fat, Tail, and Core Temperature Measurement

Brown fat tissue temperature was measured using subcutaneous implants (IPTT-300, Biomedic Data Systems, DE) inserted at the midline in the interscapular region under anesthesia at least one week before start of experiment. Measurements were taken with the non-contact DAS-7007 reader. Tail temperature was measured using an infrared thermal camera (A325, FLIR). Snapshot images were taken at the specified time points and an average of three spot readings were taken at 1 cm from base of the tail. Core temperature were taken using a thermocouple rectal probe and thermometer (Braintree Scientific, MA).

Thermal Gradient Assay

A custom thermal gradient was made from square aluminum tube (3.5 in X 3.5 in X 56 in). Mice were allowed to explore the center section (3.5 in X 3.5 in X 48 in). The cold end of the tube was encased in custom box held at $0°C$ with ice and the warm end was placed on heated surface set to $150°C$. The temperature of the gradient was allowed to equilibrate for one hour before the start of the experiment, and temperature readings at regular position intervals were checked before starting an experiment. Temperatures corresponding to each gradient position were calculated from readings taken at each position after each experiment and averaged over ten such reading sets. Subjects were recorded by video (Logitech) and the recording was analyzed for animal position across the span of the experiment at using a custom MATLAB script. All subjects were allowed to explore the pre-equilibrated gradient for one hour to establish preferred temperature before the start of light stimulation or paired icilin/light stimulation.

For paired icilin light stimulation, icilin solution was prepared fresh on the day of experiment by dilution in vehicle (0.9% sterile saline supplemented with 5% PEG400 and 5% Tween-80) and administered via intraperitoneal injection of a volume (μL) equal to 10X body weight (g), to achieve an effective dose of 5 mg/kg. Light stimulation began immediately after icilin injection. All animals engaged in vigorous grooming behavior in the first ten minutes after icilin/light stimulation so this period was excluded from analysis.

Nesting Behavior Assay

Subjects were placed in separate empty cages with a single fresh cotton fiber nestlet square (2 inch by 2 inch, Ancare) and placed at either $10°C$ or $37°C$ for 4 hr. Subjects were then returned to homecage and nestlet material was carefully removed and photographed. For nestlet traces, photograph images were imported into Adobe Illustrator software and outlines were manually traced. Outline traces were stacked to produce composite traced outlines for each group. Raw photograph images and composite traced outlines are presented.

Conditioned Place Preference Test

A custom 3-chamber apparatus was used. Floor of the two end chambers had either a grid-floor pattern or a lined-floor pattern. During the testing phases, subjects were confined to the central neutral chamber for five min then permitted to freely explore all three chambers for ten min. Chamber position was recorded by overhead video recording and analyzed by custom MATLAB script. Conditioning began 48 hr after the first testing phase. During conditioning phase, subjects were attached to optogenetic patch cable and placed in the stimulation-unpaired chamber for 15 min, and then returned to home cage. Later in the same day, animals were similarly exposed to the stimulation-paired chamber for 15 min. Stimulation (10 mW at tip, 2 Hz, 30 s) was applied five min after placement in the stimulation-paired chamber. Conditioning protocol was identical for both control and experimental subjects and repeated every 48 hr for each subject for a total of seven sessions. Post-conditioning preference test was conducted 48 hr after the last conditioning session. For CPP assay at high ambient temperature, entire protocol was performed in temperature controlled chamber so that ambient temperature during conditioing as well as pre- and post-conditioning preference tests were conducted at $38°C$. Animals were housed at regular room temperature ($20°C$) between all testing and conditioning procedures.

Acute Hypothalamic Slice Preparation and Slice Electrophysiology

Hypothalamic slices were sectioned in ice-cold oxygenated (95% O_2/ 5% CO_2) cutting saline containing (in mM) 26 $NaHCO_3$, 1.25 NaH_2PO_4, 3 KCl, 10 glucose, 210 sucrose, 2 $CaCl_2$ and 2 $MgCl_2$. Slices were then transferred to oxygenated artificial CSF (aCSF) containing (in mM) 125 NaCl, 25 $NaHCO_3$, 1.25 NaH_2PO_4, 2.5 KCl, 15 glucose, 2 $CaCl_2$ and 1 $MgCl_2$ and incubated at $34°C$ for 30 min, and recovered at room temperature for 45cmin to 1ch. During experiments, slices were placed in a recording chamber and superfused with oxygenated aCSF. Glass pipettes for recording (3–6 MΩ) were pulled from borosilicate glass capillary (O.D. 1.5 mm, I.D. 0.86 mm; Sutter Instrument). Internal solution contains (mM) 125 K-gluconate, 10 KCl, 1 EgTA, 4 Mg_3ATP_2, 0.3 Na_3ATP, 5 Na_2-phosphocreatine and 10 HEPES. Osmolarity was adjusted to 290–295cmOsm, and pH buffered at 7.3. For GCaMP6s validation slice recording, EgTA was not added in the internal solution. Whole-cell recordings were made at $32°C$ using an Axopatch 700B amplifier (Molecular Devices). Data acquisition (filtered at 5 kHz and digitized at 10 kHz) and pulse generation were performed using a Digidata 1550 and pClamp 10.5 software (Molecular Devices).

Acute hypothalamic slices were prepared from Adcyap-2A-Cre and BDNF-2A-Cre mice expressing either AAV GCaMP6s or stabilized step functional opsins (SSFO). Fluorescent cells in VMPO were identified for whole-cell patch clamp recordings at $37°C$. For

GCaMP6s virus validation, cells were activated using 30 pA step currents injected with different time intervals from 0.1 to 1.1 s under current clamp mode. For SSFO virus validation, cells were clamped at −70 mV at voltage clamp mode and −40 to −60 mV at current clamp mode. Cells were photostimulated using an LED light source (Lambda HPX, Sutter Instrument) through a 470 nm excitation filter set (U-N41017, Olympus) and 560 nm excitation filter set (U-N41004, Olympus) to activate SSFO activity by 2 Hz with 10 ms LED pulses for 30 s, or 1 s LED pulses by an Axopatch 700B amplifier (Molecular Devices).

To test their intrinsic temperature sensitivity, Pacap and adjacent non-Pacap neurons in VMPO were identified by GFP fluorescence with AAV2-EF1a-DIO-EGFP-L10a virus injection in PACAP-2A-Cre mice. By whole cell recording in acute hypothalamus slice, spontaneous firing of the cells was recorded while changing the recording temperatures by Automatic Temperature Controller (TC-324B, Warner Instrument Corporation). Synaptic blockers (10 μM CNQX and 100 μM Picrotoxin) were added into the chamber through out the whole recording. The firing frequencies were analyzed using 10 s time bins and correlated to the mean temperature for each bin. Mean firing frequency was obtained for each 0.5°C temperature range between 33°C and 40°C. To obtain normalized firing frequency, firing frequency at each temperature was expressed relative to that obtained at 36°C for the same cell.

Anterograde-Tracing

Cre-dependent rAAV expressing Synaptophysin-mCherry fusion protein (AAV9-hEF1α-DIO-Synaptophysin-mCherry) was obtained from the McGovern Viral Core Facility. 300 nL of viral aliquot was injected bilaterally into the VMPO, and subjects were sacrificed 4 weeks after injection and processed for immunohistochemistry.

Retrograde-Labeling

Recombinant Cre-dependent herpes-simplex virus expressing HA and FLAG epitope tagged ribosomal subunit L10a (HSV-hEF1α-LSL-HAFlagL10a-WPRE-SV40) was packaged at the McGovern Institute Viral Core facility using custom plasmid vectors. Virus (300 nL) was stereotaxically injected bilaterally into the DMH of BDNF-2A-Cre; Gad2-T2a-NLS-mCherry double transgenic mice. Subjects were sacrificed four weeks after injection and co-stained for mCherry and the HA epitope.

Chemogenetic Stimulation

AAV2-EF1a-DIO-hM3Dq-mcherry virus was injected into the DMH of Vglut2-IRES-Cre mice. After recovery period, DMH Vglut2 neurons stimulated by systemic treatment with synthetic ligand Clozapine-N-oxide (CNO) and the effect on BAT thermogenesis was assayed. Each trial consisted of vehicle (0.9% sterile saline supplemented with 5% PEG400 and 5% Tween-80) injection followed by CNO solution (1 mg/kg) injection two hours later. CNO was injected intraperitoneally at volume of 10X body weight (g).

Immunohistochemistry

Mice were transcardially perfused with PBS followed by formalin. Brains were postfixed overnight in formalin at 4°C and washed with PBS. Free floating sections (50 μm) were prepared with a cryostat, blocked (3% BSA, 2% NGS and 0.1% Triton-X in PBS for two hours), and then incubated with primary antibody overnight at 4°C. Sample were washed three times with (1XPBS+0.1% Triton-X), incubated with secondary antibody for two hours at room temperature, washed again and then mounted and imaged by confocal microscopy. Primary antibodies used were: anti-GFP (Abcam, ab13970, 1:1000); anti-phosphoS6(p244/p247) (Invitrogen #44923G, 1:1500), anti-RFP(Chromotek 5F8, 1:1000), anti-β-Gal (Promega #Z3783, 1:500), anti-NeuN (Millipore MAB377, 1:50).

In Situ Hybridization

ISH was performed using RNAscope assay (Cat#320293/320513, Advanced Cell Diagnostics, Manual Fluorescent Multiplex kits). Fresh whole brain was dissected from BDNF-Cre; Rosa26-LSL-GFPL10a animals and rapidly frozen in liquid nitrogen, embedded in cryo-embedding medium and sectioned on a cryostat. 20 μm sections were mounted on slides at −20°C. All subsequent steps were performed according to manufacturers instructions. Probes used: EGFP (400281-C3), Mm-BDNF (424821).

QUANTIFICATION AND STATISTICAL ANALYSIS

Statistical parameters including sample sizes (n = number of animal subjects per group), the definition of center, dispersion and precision measures, the statistical test used and statistical significance are reported in the Figures and the Figure Legends. Unless otherwise indicated, values are reported as mean ± SEM. (error bars or shaded area). *P-values* for simple pair-wise comparisons were performed using a two-tailed Mann-Whitney test. p values for all other comparisons were performed using 1-way or 2-way ANOVA followed by post hoc pair-wise comparisons using Bonferroni multiple comparisons test. All optogenetic, chemogenetic and fiber photometry trials involved age-matched littermates as controls where possible. Mice were randomly assigned before surgery to either ChR2/GCaMP or control groups. No blinding was used, but all experimental subjects were sacrificed after completion of the study and viral expression and optic fiber placement were verified by IHC, and this information was used for final assignment to experimental or control groups. No outliers were excluded from analysis. Data is judged to be statistically significant when $p < 0.05$. In figures, asterisks denote statistical significance *$p < 0.05$, **$p < 0.01$, ***$p < 0.001$, ****$p < 0.0001$. All statistical analysis was performed using GraphPad PRISM 7 software.

DATA AND SOFTWARE AVAILABILITY

Data Resources

The accession number for the raw and analyzed data files for the PhophoTRAP sequencing analysis reported in this paper is NCBI Gene Expression Omnibus: GSE80121.

The accession number for the raw and analyzed data files for the TRAP-Seq sequencing analysisreported in this paper is NCBI Gene Expression Omnibus: GSE80120.

The accession number for both datasets reported in this paper is NCBI Gene Expression Omnibus SuperSeries: GSE80224.

Supplemental Figures
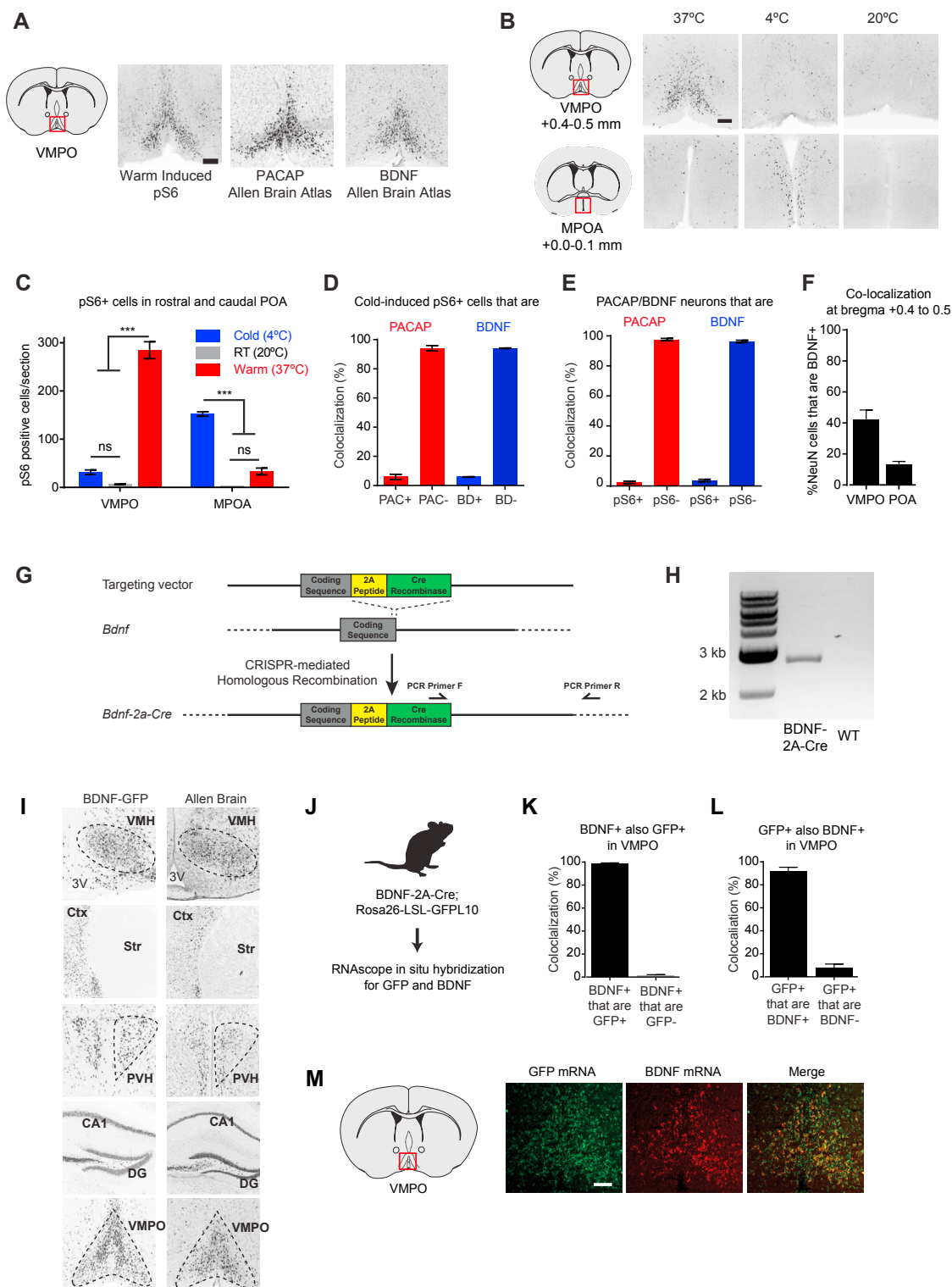
Figure S1. BDNF and PACAP Are Molecular Markers for Warm-Activated Neurons, Related to Figure 1

(A) Expression of BDNF and PACAP in the VMPO. In situ hybridization images obtained from the Allen Brain Atlas. Warm-induced activity pattern in the VMPO is shown for comparison. Scale bar = 200 μm.

(B) pS6 staining shows patterns of activation in the VMPO and MPOA after exposure to either warm (37°C, 4 h), cold (4°C, 4 h) or room temperature (20°C). Scale bar = 200 μm.

(C) Number of pS6 cells in the VMPO and MPOA after exposure to indicated temperatures. Two-way ANOVA, $F_{2,12}$(Temp X Region) = 268.7, p < 0.0001. n = 3 per group. post hoc Bonferroni multiple comparisons ***p < 0.001.

(D) Percentage of cold activated cells in MPOA that are PACAP/BDNF positive.

(E) Percentage of PACAP and BDNF cells in the VMPO that were activated in response to cold (compare with Figure 1H).

(F) Percentage of NeuN+ cells that are also BDNF+ in the VMPO and broader POA at bregma +0.4 to 0.5.

(G) Targeting vector and knock-in strategy for generating Bdnf-2a-Cre mice. Sequence encoding 2A-self cleaving peptide and Cre-recombinase are inserted before the natural STOP codon at the endogenous Bdnf allele. Primers F and R are used for PCR confirmation of site-specific homologous recombination shown in (H).

(H) Confirmation of the presence of the knock-in allele using the PCR primers shown in (G).

(I) Comparison of GFP expression in BDNF-2A-Cre; ROSA26-LSL-GFP reporter line and BDNF expression assessed by in situ hybridization obtained from Allen Brain Atlas. Strong similarity of expression was observed including expression in the ventromedial hypothalamus (VMH), cortex (Ctx), paraventricular hypothalamus (PVH), CA1 and dentate gyrus (DG) of the hippocampus and in the ventromedial preoptic hypothalamus (VMPO).

(J–M) In situ hybridization (ISH) experiments demonstrate overlap between recombinase activity in BDNF-2A-Cre animals and endogenous Bdnf gene expression. (J) Double transgenic animals BDNF-2A-Cre; Rosa26-LSL-GFPL10a was used for ISH for GFP and BDNF mRNA. (K and L) Bar graphs quantify percentage of BDNF+ cells that express GFP (K) and percentage of GFP+ cells that express BDNF (L). (M) Representative ISH image for endogenous BDNF mRNA and GFP mRNA in BDNF-2A-Cre; ROSA26-LSL-GFP mice. Scale bar = 100 μm.
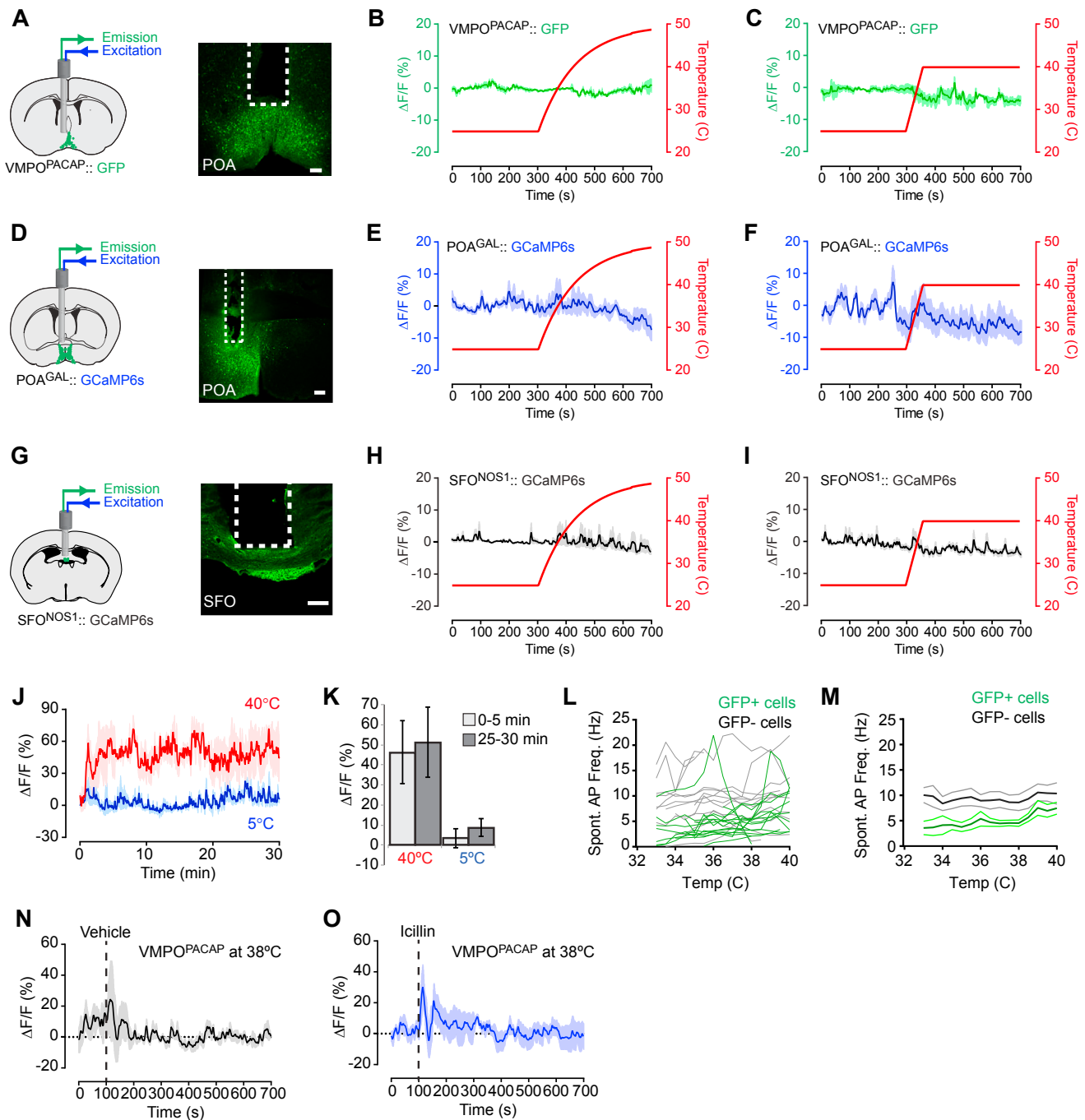
Figure S2. Fiber Photometry of VMPO^{PACAP} Neurons, Related to Figure 2

(A–I) No responses to warm temperatures were observed in either VMPO^{PACAP} cells expressing GFP (A-C, green; scale bar = 100 µm), Galanin neurons in the POA expressing GCaMP6s (D-F, blue; scale bar = 200 µm) or Nos1 neurons in the subfornical organ expressing GCaMP6s (G-I, black; scale bar = 100 µm). (A,D,G) show anatomic location of targeted cell groups and representative coronal slices show expression of GFP or GcaMP6s as well as fiber placement (white dotted lines). Increasing temperatures (red line) were applied in either slow ramp (B,E,H) or in rapid step (C,F,I). Line graphs show mean fluorescence response ± SEM. (J and K) Response to warmth is long-lasting and stable. (J) Fluorescence response as temperature is changed rapidly (~60 s) at time = 0 from 25°C to 40°C (red) or from 25°C to 5°C (blue) and kept at target temperature for 30 min. (K) Bar graphs show mean response between t = 0 and t = 5 min and between t = 25 and t = 30 min after temperature challenges shown in (J). Two-way ANOVA, $F_{1,8}$(Temp) = 12.29, p = 0.008; $F_{1,8}$(Time) = 0.17, p = 0.68.

(L and M) No differences in cell-intrinsic temperature sensitivity between POA^{PACAP} and adjacent VMPO neurons. Spontaneous action potential firing rate was obtained from whole cell recordings of VMPO^{PACAP} neurons (GFP+, green, n = 15, 7 mice) and non-PACAP expressing neurons (GFP-, gray, n = 14, 7 mice). Lower spontaneous AP firing was observed in POA^{PACAP} neurons [two-way ANOVA $F_{1,298}$(Group) = 74.45, p < 0.001], but no significant effect of bath

(legend continued on next page)

temperature was found [two-way ANOVA $F_{16,298}$(Interaction) = 0.2553, p = 0.99; $F_{16,298}$(Temperature) = 0.9, p = 0.56]. (L) Recordings from individual cells (M) Group mean ± SEM.

(N and O) Icilin does not inhibit VMPO^{PACAP} neuron activity even after preactivation by high ambient temperature. Chamber temperature was raised from room temperature to 38°C resulting in increased fluorescence response (data not shown). 15 min later, animals were challenged with vehicle (N) and then Icilin (O) injections. Line graphs show responses normalized to mean fluorescence after paired vehicle injection.
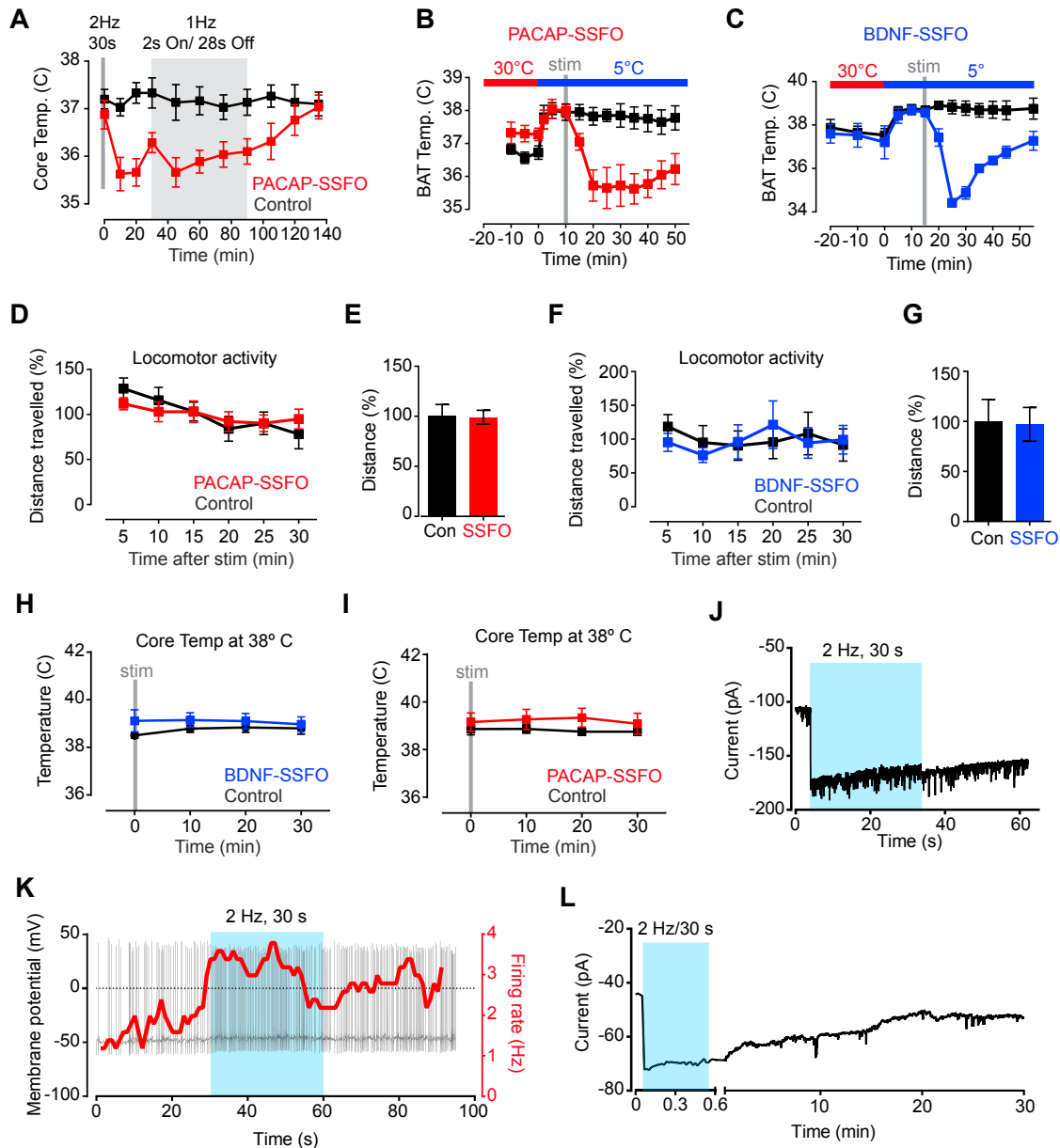
Figure S3. Optogenetic Activation of VMPO$^{PACAP/BDNF}$ Neurons Results in a Durable Decrease in Body Temperature and Reverses Cold-Induced Autonomic Responses, Related to Figure 3
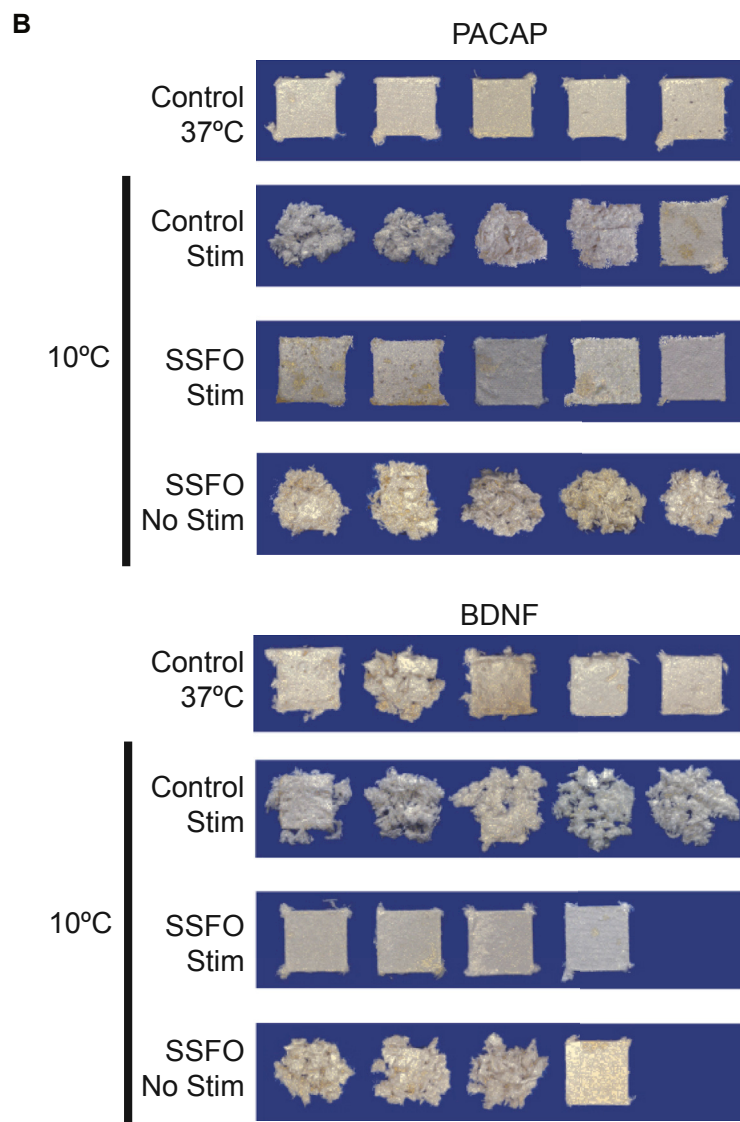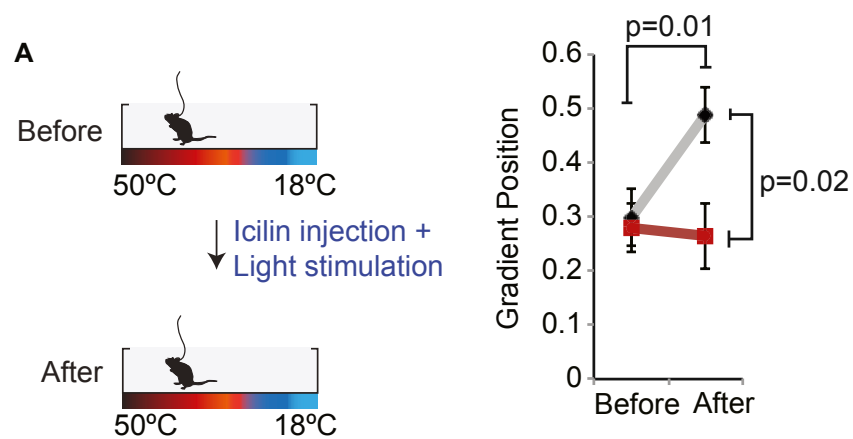
(A) Core body temperature is lowered by a single burst of light stimulation (2 Hz, 30 s at t = 0 min) and this is maintained during persistent low-frequency stimulation (1 Hz, 2 s-ON/28 s-OFF, from t = 30-90 min). Line graph shows mean ± SEM.

(B and C) VMPO$^{PACAP/BDNF}$ neuron stimulation (SSFO) reverses cold-induced brown fat thermogenesis. Temperature decrease (30°C to 5°C), prior to stimulation, induces robust brown fat temperature increase in all subject groups. Subsequent light stimulation (2Hz, 30 s) of VMPO^{PACAP} (B, red) or VMPO^{BDNF} (C, blue) neurons induced reductions in brown fat temperature even at 5°C. Two-way RM-ANOVA, Group X Time interaction. $F_{11,77}$(PACAP) = 8.42, p < 0.001; $F_{7,49}$(BDNF) = 25.70, p < 0.001.

(D–G) SSFO-mediated stimulation of PACAP (D-E, red) or BDNF (F-G, blue) cells does not alter locomotor activity. Line graphs show mean distance traveled in each 5 min window after light stimulation (2 Hz, 10 mW, 30 s). Bar graphs shows mean total distance traveled in the first 30 min following stimulation. Two-tailed Mann Whitney test PACAP = 0.61, BDNF = 0.93. n = 5-9. All values expressed relative to control mean.

(H and I) Concurrent exposure of mice to ambient heat (38°C) beginning one hour before light stimulation occludes core body temperature reductions induced by light-stimulated VMPO$^{PACAP/BDNF}$ neuron activity. Compare to Figure 3D. Two-way RM-ANOVA, All factors p > 0.05. n = 5-6.

(J–L) Optical stimulation of PACAP neurons expressing SSFO in slice results in sustained depolarization and increased spontaneous firing. (J,K) Stimulation of PACAP-SSFO neurons in slice with the same pulse sequence used in vivo (2 Hz, 30 s, 10 mW) results in inward current and increased firing rate. Red line is a 5 s sliding average of the spontaneous firing rate. (L) Inward current induced by optical stimulation of PACAP-SSFO neurons persists for tens of minutes in vitro, as previously reported.

A

Before

50ºC   18ºC

Icilin injection +
Light stimulation

After

50ºC   18ºC

p=0.01

p=0.02

Gradient Position

0.6
0.5
0.4
0.3
0.2
0.1
0

Before   After

B

PACAP

Control
37ºC

Control
Stim

10ºC

SSFO
Stim

SSFO
No Stim

BDNF

Control
37ºC

Control
Stim

10ºC

SSFO
Stim

SSFO
No Stim

(legend on next page)

Figure S4. Optogenetic Activation of VMPO^{PACAP/BDNF} Neurons Stimulates Behavioral Thermoregulation, Related to Figure 4

(A) VMPO^{PACAP} neuron stimulation reverses icilin-induced heat-seeking. Left: Schematic, thermal gradient assay is used to assess temperature preference. Light stimulation (2 Hz, 30 s) and icilin injection (5 mg/kg IP) are applied simultaneously. Right: Median gradient position in the 15 min period before and after icilin/light stimulation is shown. n = 5-8 per group. p values: 2-tailed unpaired t test.

(B) Nesting building activity is inhibited by warm temperature and by VMPO$^{PACAP/BDNF}$ neuron stimulation. Photographs of square nestlets after 4 hr nesting activity trial at either 10°C or 37°C are shown. Stimulation was applied at 2 Hz for 10 s every 30 min. Control-Stim and SSFO-Stim images are identical to those shown in Figure 4E.
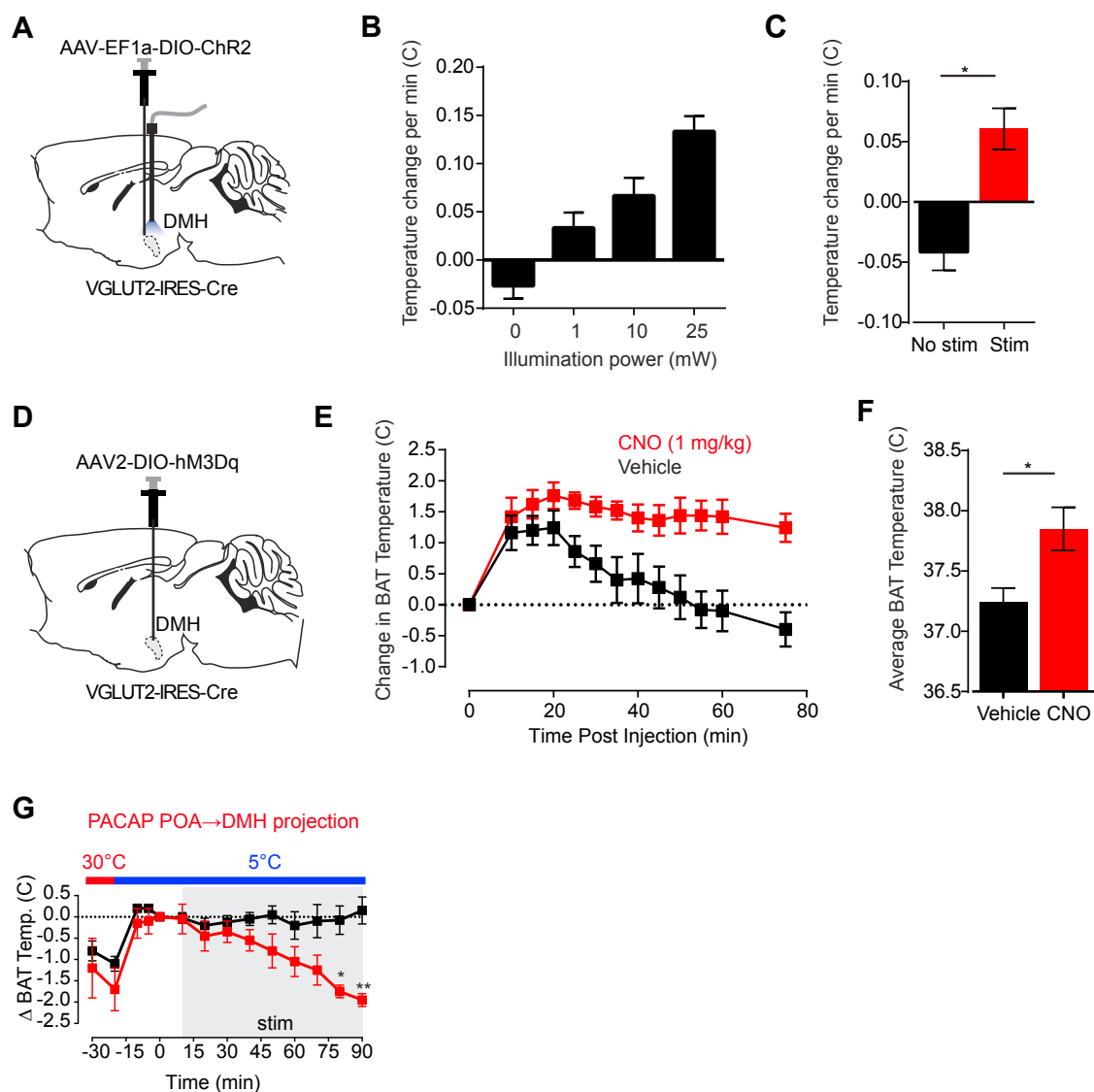
Figure S5. VMPO^PACAP Projection to DMH Inhibits BAT Thermogenesis, Related to Figure 7

(A–C) Optogenetic stimulation of glutamatergic DMH neurons. (A) Schematic of optogenetic stimulation. A Cre-dependent AAV expressing ChR2(H134R) was injected into the DMH of VGLUT2-IRES-Cre mice. An optical fiber was implanted above the DMH and animals were stimulated at 10 Hz at the powers indicated with a 1 s ON:1 s OFF duty cycle. (B) Average rate of change of brown fat temperature is shown at each illumination power. (C) Average rate of change of brown fat temperature in the presence or absence of stimulation (all illumination intensity > 5 mW is pooled). n = 2 per group.

(D–F) Chemogenetic stimulation of glutamatergic DMH neurons. (D) Schematic of chemogenetic strategy. Cre-dependent AAV-virus expressing excitatory DREADD receptor (hM3Dq) was injected into the DMH of VGLUT2-IRES-Cre animals. Brown fat temperature was recorded after IP injections with either vehicle or synthetic DREADD ligand clozapine-N-oxide (CNO; 1 mg/kg). (E) Change in BAT temperature relative to pre-injection (0 min) after IP injection of vehicle or CNO. Note that vehicle injection results in a transient increase in BAT temperature as a result of animal handling and stress, but that the elevation of BAT temperature following CNO injection is sustained. (F) Average BAT temperature in 75 min period after injection. n = 5.

(G) ChR2-mediated stimulation of DMH projections of POA^PACAP neurons reverses cold-induced BAT thermogenesis. Change in BAT temperature is shown relative to start of stimulation period (gray) Two-way RM-ANOVA, $F_{17,204}$(Group X Time) = 1.746, p < 0.05. n = 4-10.

All values show mean ± SEM 2-tailed Mann Whitney test. *p < 0.05, **p < 0.01.